Biogeosciences

Methane in Zackenberg Valley, NE Greenland: multidecadal growing season fluxes of a high-Arctic tundra

Johan H. Scheller[1,2], **Mikhail Mastepanov**[1,3], **Hanne H. Christiansen**[2], and **Torben R. Christensen**[1,3]

[1]Department of Ecoscience, Arctic Research Centre Aarhus University, Roskilde, Denmark
[2]Arctic Geology Department, The University Centre in Svalbard, Longyearbyen, Norway
[3]Oulanka Research Station, University of Oulu, Oulu, Finland

Correspondence: Johan H. Scheller (jscheller@ecos.au.dk)

Abstract. The carbon balance of high-latitude terrestrial ecosystems plays an essential role in the atmospheric concentration of trace gases, including carbon dioxide (CO_2) and methane (CH_4). Increasing atmospheric methane levels have contributed to $\sim 20\%$ of the observed global warming since the pre-industrial era. Rising temperatures in the Arctic are expected to promote the release of methane from Arctic ecosystems. Still, existing methane flux measurement efforts are sparse and highly scattered, and further attempts to assess the landscape fluxes over multiple years are needed.

Here we combine multi-year July–August methane flux monitoring (2006–2019) from automated flux chambers in the central fens of Zackenberg Valley, northeast Greenland, with several flux measurement campaigns on the most common vegetation types in the valley to estimate the landscape fluxes over 14 years. Methane fluxes based on manual chamber measurements are available from campaigns in 1997, 1999–2000, and in shorter periods from 2007–2013 and were summarized in several published studies. The landscape fluxes are calculated for the entire valley floor and a smaller subsection of the valley floor, containing the productive fen area, Rylekærene.

When integrated for the valley floor, the estimated July–August landscape fluxes were low compared to the single previous estimate, while the landscape fluxes for Rylekærene were comparable to previous estimates. The valley floor was a net methane source during July–August, with estimated mean methane fluxes ranging from 0.18 to 0.67 mg m^{-2} h^{-1}. The mean methane fluxes in the fen-rich Rylekærene were substantially higher, with fluxes ranging from 0.98 to 3.26 mg m^{-2} h^{-1}.

A 2017–2018 erosion event indicates that some fen and grassland areas in the center of the valley are becoming unstable following pronounced fluvial erosion and a prolonged period of permafrost warming. Although such physical disturbance in the landscape can disrupt the current ecosystem–atmosphere flux patterns, even pronounced future erosion of ice-rich areas is unlikely to impact methane fluxes on a landscape scale significantly. Instead, projected changes in future climate in the valley play a more critical role. The results show that multi-year landscape methane fluxes are highly variable on a landscape scale and stress the need for long-term spatially distributed measurements in the Arctic.

1 Introduction

It was recognized early in climate change research that the Arctic is particularly prone to increasing temperatures, and considerable changes to ecosystems at high latitudes were to be expected (IPCC, 1990). For decades, hence, tundra ecosystems have been subject to attention concerning changing climate. Further, high-latitude wetlands have, for a long time, been recognized as a contributor to the global atmospheric budget of methane (CH_4). In the first global budget, the tundra source was an estimated 1.3 to 13 Tg yr^{-1} of a total atmospheric burden of 529 to 825 Tg yr^{-1} (Ehhalt, 1974). This term and the overall atmospheric budget have changed remarkably little during nearly 50 years of research, with emission estimates for all global wetlands ranging from 140 to 280 Tg yr^{-1} in the 1970s as well as in the 2010s (Christensen, 2014). This still also forms the background for

the concern that with Arctic ecosystems warming, the so far modest wet tundra emissions may increase and start a positive feedback in the climate system (Knoblauch et al., 2018). In addition to Arctic warming, landscape changes such as permafrost thaw affecting tundra ecosystems and lake formations have been identified as possible hotspots for increased emissions (Schuur et al., 2015; Walter Anthony et al., 2018). Also, coastal and further offshore marine sources are subject to possible changed emissions in the Arctic (Shakhova et al., 2014; Thornton et al., 2020), but these are not dealt with here. Overall, these concerns led to early and still continuing efforts at quantifying more closely the Arctic natural emissions and their sensitivity and dynamics in relation to climate change.

Studies of tundra methane emissions in several parts of the Arctic were initiated between the 1970s and 1990s (Svensson and Rosswall, 1984; Whalen and Reeburgh, 1988; Morrissey and Livingston, 1992; Christensen, 1993). Zackenberg Valley in northeast Greenland was one of the first high-Arctic sites to be added to the circumpolar map of methane flux studies in 1997 (Christensen et al., 2000) after the start of the Zackenberg Ecological Research Operations (ZERO) in 1995 (Meltofte et al., 2008). Since then, the valley has seen several different methane flux studies, and methane monitoring became part of the Greenland Ecosystem Monitoring (GEM) program in 2007 (Mastepanov et al., 2013). With numerous short-term research projects, the monitoring has led to the availability of a unique, large number of years with observations of fluxes compared to any other location in the Arctic.

The overarching background for the sizeable emissions in the Arctic is that waterlogged undisturbed soil environments host stable anaerobic environments with optimal conditions for methanogenic activity. Compared with tropical wetlands influenced heavily by the seasonality of flooding (Nisbet et al., 2019), the arctic source areas tend to be more stable geographically. Their emissions are subject to the balance between the production at depth and the microbial oxidation in the aerobic surface layer. However, through recent decades, many factors such as nutrients, plant species composition, and topography/hydrology have been found to influence the size of the emissions (AMAP, 2015). From a landscape perspective, the constantly emitting wet soil environments are surrounded by and intermixed with uplands, glaciers, lakes, and rivers, all with their distinct and, in some cases, very different methane flux characteristics. It is rare that a comprehensive analysis of both these small-scale controls and spatial heterogeneity is possible simply due to a lack of locations where enough studies of different kinds of land cover have been conducted. Zackenberg Valley is here unique, with such a wide range of studies available.

Here we compile all methane flux studies conducted so far in Zackenberg Valley with the objectives to (1) review the combined information from these studies on temporal and spatial variability of methane fluxes in a composite high-

Arctic landscape and (2) assess the sensitivity of the measured fluxes as they respond to climate warming or local changes. A large number of studies and multiple years of observations, along with the addition of flux measurements from a recent gully, provide a unique opportunity to disentangle the effect of different processes and quantify their relative influence on the fluxes on a landscape scale. These processes can broadly be grouped as (1) climate variability and the projections for a gradual warming and (2) increased erosion of vegetated surfaces.

The challenge is to quantify the sensitivity of the landscape fluxes to these factors individually to allow for quantitative analysis of how the factors combine and compare in terms of sensitivity to established climate warming scenarios. To conduct this study, we use a combination of published data and new measurements of methane fluxes from a recently eroded gully near the Zackenberg Research Station and its immediate surroundings.

2　Materials and methods

2.1　Site description

2.1.1　Study area

Zackenberg Valley is located at 74.47° N, 20.55° W in northeast Greenland. The study area follows the boundaries used in Søgaard et al. (2000) and covers the core monitoring and research projects area of the GEM program (Zone 1A) below 200 m above sea level, encompassing a total area of $\sim 16\,\text{km}^2$ on the valley floor (Fig. 1). The vegetated areas consist of continuous and hummocky fens, grasslands, *Salix* snowbeds, and *Cassiope* and *Dryas* heaths. Common species in the fens include *Dupontia psilosantha* and *Eriophorum scheuchzeri*, and graminoids, including *Arctagrostis latifolia*, *Eriophorum triste*, and *Alopecurus alpinus*, cover the grassland areas (Bay, 1998).

Rylekærene partly covers the valley floor study area and consists of a $1.3\,\text{km}^2$ patterned wet tundra ecosystem dominated by fen areas and divided by drier patches of heaths and grasslands in the central part of the valley (Tagesson et al., 2013). Rylekærene has been a subject of several methane flux studies since the mid-1990s, and several sites within the area have been in use (Fig. 1).

A backward erosion gully, previously referred to as "thermokarst" (Christensen et al., 2020b), extends from Gadekæret, a small fen area close to Zackenberg Research Station in the central part of the valley (Fig. 1). The dendritically shaped gully formed rapidly during July 2018, most likely triggered by substantial lateral erosion of up to 4.7 m in an outer bend of the river after a glacier lake outburst flood (GLOF) in August 2017 (Tomczyk et al., 2020). The gully is up to 1 to 4 m deep, up to 8 m wide, and $\sim 50\,\text{m}$ long in the longest flow direction. This process is different
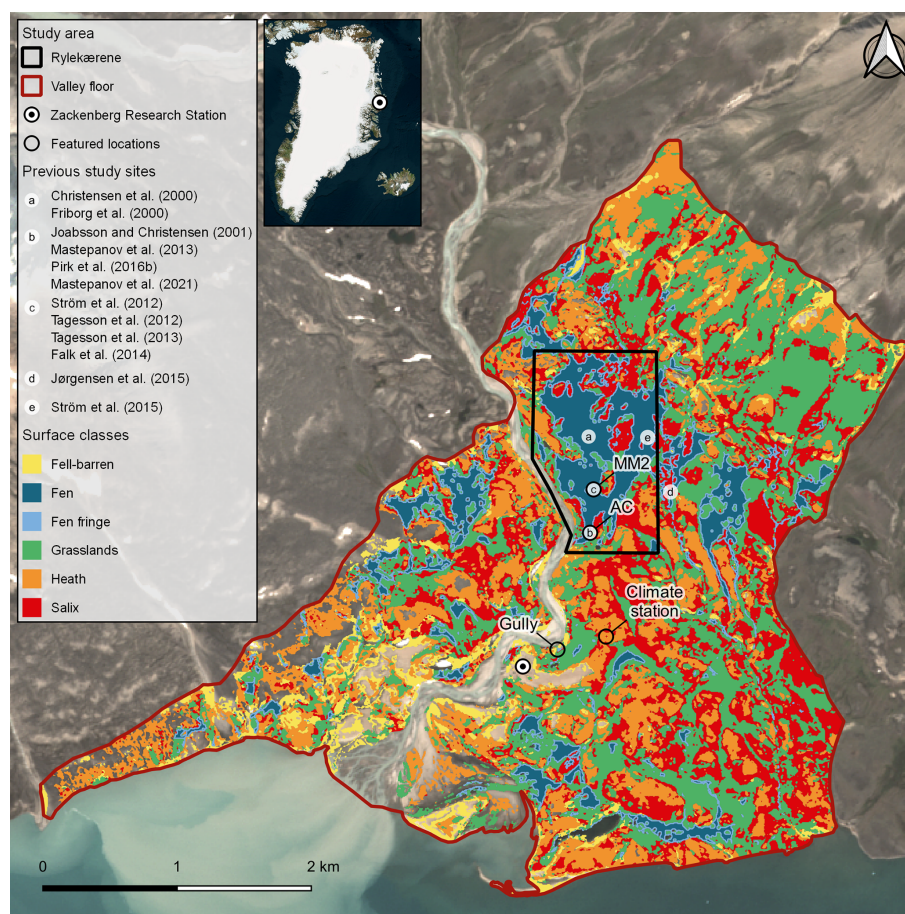
Figure 1. The study area with dark red and black boundaries showing the valley floor study area and Rylekærene in Zackenberg Valley (74.47° N, 20.55° W) and approximate locations of previous study sites are marked with letters. The two gas flux monitoring sites, AC and MM2, are found at the same places as study sites b and c, marked with black circles. Colored areas show the spatial distribution of the six surface classes used in this study. Data sources: HyMap hyperspectral imaging campaign (7 August 2000) (Elberling et al., 2008), ESA Copernicus Sentinel-2 (16 July 2019), and © BING Maps 2021.

from thermokarst and is similar to the active development of a gully in the northern part of Zackenberg Valley in 1999 (Christiansen et al., 2008). The retrogressive, branching pattern of the gully likely occurs along with ice wedges in the area. Meltwater from a large snowpack in Gadekæret in early 2018 has most likely saturated the thawed sediments and thermally eroded the ice wedges, causing sediment transport from the site and into the river.

The gully was monitored closely during the 2019 field season, but its development had ceased. Standing water covered the bottom of the gully during August 2018, and elevated methane concentrations were detected in the area (Christensen et al., 2020b). In 2019, the bottom of the gully had dried out, and methane concentrations were no longer elevated.

Table 1 shows the coverage of each surface class compared to the valley floor and Rylekærene areas in both absolute and relative terms, based on hyperspectral aerial data from Elberling et al. (2008), which improved on a manual land cover

classification by Bay (1998). Zackenberg River has changed its course since 2000 after multiple GLOF events (Søndergaard et al., 2015; Tomczyk and Ewertowski, 2020), and we adjusted the land cover classification map to fit the extent of the river in a 2014 orthomosaic of the entire study area (COWI, 2015).

2.1.2 Climatology

The study area is defined as high Arctic (Meltofte and Rasch, 2008), with mean annual air temperature and precipitation of $-8.6\,°C$ and 253 mm (2008–2018) (López-Blanco et al., 2020). Continuous permafrost underlies the valley (Christiansen et al., 2008), and the active layer (AL) reaches a maximum depth of 0.58 to 0.85 m, increasing at a rate of $0.74\,cm\,yr^{-1}$ (1996–2019) at the ZEROCALM-1 site (Christensen et al., 2020a) near the climate station at the valley floor.

Table 1. Absolute and relative area distributions for the six main surface cover classes in the two study areas shown in Fig. 1, updated to the Zackenberg River extent in 2014. The "fen fringe" surface class covers the outer 10 m of the fen areas.

Surface class	Valley floor in m^2 (% of the area)	Rylekærene in m^2 (% of the area)
Fens	983 920 (6.2 %)	464 816 (36.6 %)
Fen fringes	920 504 (5.8 %)	176 502 (13.9 %)
Grassland	4 429 921 (27.9 %)	176 135 (13.9 %)
Fell and barren	964 643 (6.1 %)	7854 (0.1 %)
Heaths	3 434 361 (21.6 %)	138 692 (10.9 %)
Salix snowbeds	3 244 606 (20.4 %)	265 979 (20.9 %)
Other	2 891 691 (18.1 %)	41 325 (3.7 %)
Total	15 905 003 (100 %)	1 271 303 (100 %)

2.2 Methane flux measurements

2.2.1 Measurements in Rylekærene

The first methane flux measurements in Rylekærene were carried out in 1997 in Christensen et al. (2000) and Friborg et al. (2000). They used manual flux chamber measurements and the eddy covariance (EC) method in the center of the fen area (Fig. 1, site a). In the south end of Rylekærene, Joabsson and Christensen (2001) measured methane fluxes in 1999–2000 (Fig. 1, site b). An automated chamber setup was added nearby in 2005. The automated chambers (ACs) measure methane and CO_2 fluxes along a topographic gradient from a wet fen to a heath area. The AC site is a part of the GeoBasis subprogram of GEM (Mastepanov et al., 2008, 2013).

Tagesson et al. (2012) measured methane and CO_2 fluxes by gradient EC methods at a site in the center of Rylekærene in 2008 and 2009. This site (Fig. 1, site c) is located ~ 250 m north of the AC site and was later promoted to a permanent EC CO_2 flux installation for measurements in the GeoBasis subprogram under the MM2 (MicroMet 2) name (Lund et al., 2008–2011; Stiegler et al., 2016).

In 2007, Tagesson et al. (2013) measured methane fluxes of the most common vegetation types in a ~ 600 m^2 area in the center of Rylekærene, 50 to 150 m east of the current location of MM2.

More recently, several studies focused on areas outside the permanent AC and MM2 sites, including Jørgensen et al. (2015) (Fig. 1, site d) and Ström et al. (2015) toward the eastern border of Rylekærene (Fig. 1, site e). The length of these campaigns, their onset compared to the beginning of the growing season, the sampling area, and strategy vary between studies. Figure 2 shows a timeline of methane flux campaigns from published studies and data from the GEM database.

Most of the previous studies in the research area were based on mobile flux chambers and stationary automatic chambers, which utilized changes in methane concentration measured over time inside a closed chamber to estimate surface fluxes. The chamber was sealed off to all sides but the bottom during each measurement, isolating the flux estimates to a specific time and area, analogous to the approach described by, e.g., Crill et al. (1988) and Livingston and Hutchinson (1995). Methods vary between the studies, with differences in gas analyzers, chamber designs, measurement time, replication numbers, sampling frequency, and the length of the study periods. Details on the methods are summarized in Table 2.

For the aims of the current study, we combined existing data of growing season methane from the studies shown in Fig. 2 from 2006 and forward. Only parts of the AC flux time series were used in this study; the July–August flux includes the peak of the growing season in the valley, and it matches the timing of most of the previous studies.

2.2.2 Measurements in the gully area

We conducted 113 measurements from 23 August to 1 September 2019 in a grid covering the recent gully and extending toward a small lake in the Gadekæret fen area, close to Zackenberg Research Station (Fig. 4).

The measurements took place between 09:00 and 19:00 UTC on 43 plots located 4 to 5 m from each other in the three main surface classes in the area: fens, grasslands, and in the gully. Several flux measurements at each surface class were performed every day.

A metal collar was carefully installed on the ground on each plot; a dark acrylic chamber was placed over the collar for a minimum of 5 min. The footprint of the collar was 0.07 m^2; the height from the soil surface to the top of the chamber was recorded for each measurement. The height ranged from 0.26 to 0.48 m, depending on the surface topography. The chamber was equipped with a fan inside and had a 3 mm vent on the side. A gas analyzer (Ultraportable Greenhouse Gas Analyzer, Los Gatos Research, USA) was connected to the chamber with a pair of 15 m long HDPE tubes. The gas analyzer was continuously measuring methane concentration in the chamber headspace at 1 Hz frequency. After each sample, the chamber was ventilated for at least 2 min until the methane concentration was down to ambient concentration.

2.3 Data processing

2.3.1 Environmental changes

Monitoring of air (2 m above ground) and soil temperature (0.20 m below ground) were summarized from 1997–2019 data (60 min resolution) from the nearby climate station (Fig. 1), operated by the GEM ClimateBasis program. Mean
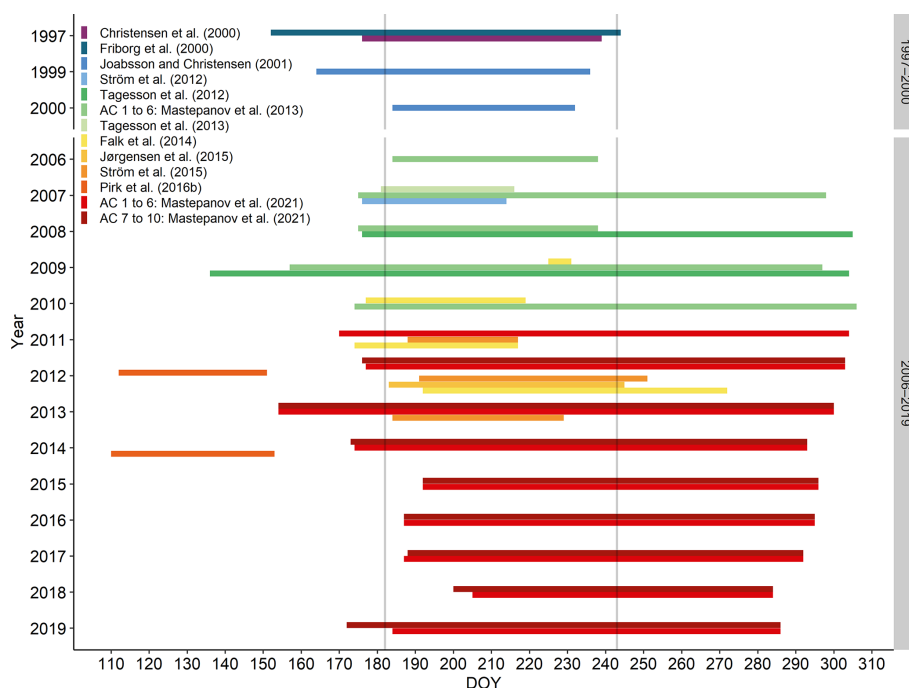
Figure 2. Timeline of methane measurement campaigns and monitoring in individual years, shown as the day of year (DOY). Colors show different publications, and the two vertical gray bars show 1 July and 31 August in non-leap years. Please note that the years 2001–2005 are left out, as no published studies focusing on methane fluxes in undisturbed areas were made in this period.

temperatures are calculated for July–August data (Fig. 3a). The day of 20 % snow cover in the central valley is available from Pedersen et al. (2016) for the 1999–2014 period (Fig. 3b). Day of 20 % snow cover is estimated from GeoBasis monitoring data for 2015–2019. Soil moisture data at the heath site Mix-1, monitored under the GeoBasis program, were summarized as mean soil moisture percentage with SD for July–August (Fig. 3c). Water level data were collected manually daily at the AC site chamber 1 from 2006–2019. Automatic water level data are collected for 2010–2019, with a gap in data in 2013 at two sites, one near chamber 1 and another near chamber 6, positioned slightly higher in the terrain. The mean water levels are calculated for July–August (Fig. 3d), and SD is omitted to improve the readability of the figure. Dataset specifications are available from the links under "Code and data availability".

2.3.2 Measurements from automated and manual chambers

Data from several sources were included in the calculation of a timeline of landscape fluxes in Zackenberg Valley. Previously published and unpublished data were compiled to estimate fluxes and standard error (SE) on the six surface types (Table 3), combining mobile flux measurements and flux measurements from AC. The measurement methods are described in detail in their respective publication, but for the AC, additional steps were added after applying the same ap-

proach as Mastepanov et al. (2013). The AC flux time series was separated into two datasets. One dataset represents a long time series from a 10 m wide transition zone at the fen fringe (chambers 1 to 6). In this area, chambers with higher numbers are generally drier. Another time series represents the changes since 2012 in the four outer chambers, located further out into the fen (chambers 7 to 10). The flux data do not show a diurnal pattern for July and August, so all available data were used in those 2 months. The flux measurements were first averaged for each chamber. Mean chamber fluxes were then further averaged into a single mean methane flux for each year for all the six inner chambers. The same was done for the four outer chambers from 2012–2019.

In 2006, only four chambers were operating, and no data were available for chambers 4 and 6. Potential differences in methane flux are corrected by multiplying the mean of the available 2006 data by a coefficient based on 2007 data. This coefficient was found by dividing the mean in chambers 1, 2, 3, and 5 by the mean of all six chambers.

Fen flux

The mean July–August flux for chambers 7 to 10 was then combined with the mean growing season fluxes from the other studies listed in Table 3. In the valley-wide vegetation cover map, hummocky and continuous fens were not separated into different classes, even though mean fluxes differ substantially for these two surface types in, e.g., Ta-

Table 2. Flux chamber measurements in Zackenberg Valley vary in several ways between studies. Please see each study for a detailed description of the methods. Only the data used in this study are included in the table, i.e., unmanipulated and control plots.

Publication and study year	Gas analysis	Chamber design	Sampling time	Plots	Measurement frequency
Christensen et al. (2000) in 1997	Duplicate syringe sample in two 10 to 15 min intervals; analysis with a Shimadzu GC14-B gas chromatograph	13 to 30 L, aluminum dark chambers on bases permanently inserted to 10 to 20 cm depth	20 to 30 min	30 plots in five sites	Two times per week
Joabsson and Christensen (2001) in 1999–2000	Duplicate syringe samples were taken at regular intervals; analysis with a Shimadzu GC14-B gas chromatograph	14 to 22 L, aluminum dark chambers on permanently installed bases (15 cm depth)	NA	Six plots in one site (only control plots)	One to three times per week
Ström et al. (2012) in 2007	LGR DLT200 analyzer	2.2 L, transparent chamber on permanently installed aluminum bases ("set-up[1]")	3 min	15	Two to four days interval
Mastepanov et al. (2013) in 2006–2010, Mastepanov et al. (2021) in 2011	LGR DLT100 model 908-0007	~ 108 L permanently installed transparent, automatic chambers	5 min	Four (2006) Six (2007–2011)	Every hour
Tagesson et al. (2013) in 2007	LGR DLT200 analyzer	10 L, transparent chamber inserted into ~ 2 cm notches in the ground	3 min	55 plots in seven sites	Two to three times per week
Falk et al. (2014) in 2009–2012	LGR DLT200 analyzer and Gasmet Dx 40-30 Fourier transform infrared spectrometer	41 L, transparent and dark chambers on bases permanently installed to 15 cm depth	3 to 7 min	15 plots in one site (only unmanipulated plot)	Approximately two times per week
Jørgensen et al. (2015) in 2012	LGR DLT100 analyzer	Volume NA, transparent and dark chambers on permanent bases inserted to ~ 10 cm depth	10 min	40 plots in four sites	NA, 280 samples in total during four campaigns
Ström et al. (2015) in 2011–2013	Gasmet Dx 40-30 Fourier transform infrared spectrometer	41 L, transparent and dark chambers on bases permanently installed to 15 cm depth	3 to 7 min	16 to 20	Approximately two times per week
Pirk et al. (2016b) in 2012 and 2014, Mastepanov et al. (2021) in 2012 to 2019	LGR Greenhouse Gas Analyzer model 908-0011	~ 108 L permanently installed transparent automatic chambers	5 min	10	Every 90 min

ble 3 in Tagesson et al. (2013) and Table 1 in Christensen et al. (2000).

Each mean flux measured in fen areas was paired with the mean flux measured at the fen fringe. Using R (R Core Team, 2021), we applied unweighted Deming linear regression on the data ($n = 18$, jackknife method, error ratio $= 0.44$, Pearson's $r = 0.64$, p-value threshold $= 0.05$). The approach accounts for uncertainties in both the fen fringe data and in the fen data to estimate a time series for the fen surface types for 2006–2019. The measurements used in the regression for the fen areas are summarized in Table 3.

Fen fringe flux

The mean flux from the fen fringes was estimated from the mean July–August flux measured every year in the 2006–2019 period using all the available data from chamber 1 to 6 (Table 3). The timeline of mean fluxes at the fen fringe represents the outer 10 m of all fen surfaces in the valley, shown in Fig. 1 without further processing.
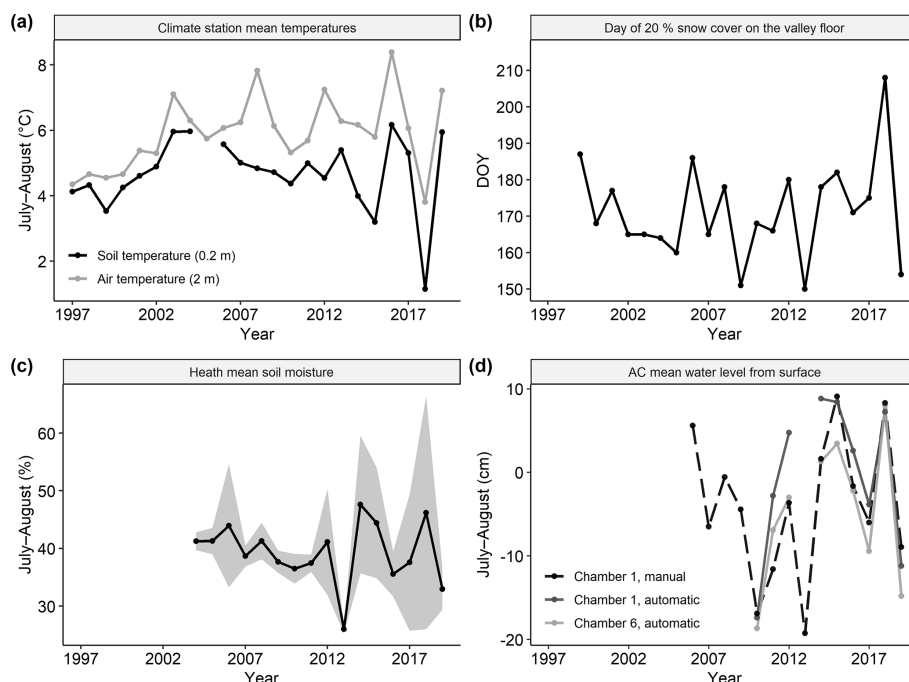
Figure 3. (a) July–August mean temperatures measured at the Zackenberg climate station. **(b)** Timing of 20 % remaining snow cover on the valley floor with 1999–2014 data from Pedersen et al. (2016). **(c)** July–August mean soil moisture at the Mix-1 heath site in the lower valley with standard deviation (SD) as shading. **(d)** July–August mean water level relative to the surface measured close to chamber 1 and chamber 6 at the AC site. Data sources: GEM ClimateBasis and GeoBasis Zackenberg.

Table 3. Summary of data and processing used in the calculation of landscape methane fluxes for the six surface classes.

Surface class	Data source	Measurement year(s)	Processing
Fens	Ström et al. (2012) ($n = 210$) Tagesson et al. (2012) Tagesson et al. (2013) ($n = 162$) Falk et al. (2014) ($n = 35$–85) Ström et al. (2015) ($n = 80$–140) Mastepanov et al. (2021) ($n = 1465$–3432)	2007 2008–2009 2007 2010–2012 2011–2013 2012–2019	Fit mean fluxes to fen fringe time series using Deming linear regression, paired by year, SE estimates from jackknife method
Fen fringes	Mastepanov et al. (2013) ($n = 3713$–8238) Mastepanov et al. (2021) ($n = 1888$–4837)	2006–2010 2010–2019	July–August means for chamber 1–6, SE calculated from variability in flux measurements
Grasslands	Tagesson et al. (2013) ($n = 110$)	2007	Constant mean flux of grasslands, SE calculated from reported SD and n
Fell and barren	Jørgensen et al. (2015) ($n \sim 140$)	2012	Constant mean flux of dry tundra, SE calculated from reported SD and n
Heaths	Christensen et al. (2000) ($n \sim 90$) Tagesson et al. (2013) ($n = 162$) Jørgensen et al. (2015) ($n = 280$)	1997 2007 2012	Constant mean flux of *Dryas/Cassiope/Vaccinium* heaths and moist/dry tundra flux, first weighted average by study, pooled SE
Salix snowbeds	Christensen et al. (2000) ($n \sim 42$) Tagesson et al. (2013) ($n = 51$) Jørgensen et al. (2015) ($n \sim 140$)	1997 2007 2012	Constant mean flux of all *Salix* snowbed surfaces, and moist tundra flux, pooled SE

Grassland flux

The grassland fluxes are held constant over the time series, with data from Tagesson et al. (2013) as input to the calculation (Table 3), while grassland fluxes from Christensen et al. (2000) are omitted due to high spatial variability and a higher average flux.

Fell and barren fluxes

Jørgensen et al. (2015) found a significant methane uptake on unvegetated fell and barren surfaces in Zackenberg Valley in 2012. These measurements were grouped into a broader "dry tundra" class that includes *Dryas* heath. Here, we use the mean methane flux from the dry tundra class but only applying it for the fell and barren areas. The mean flux from these surfaces is held constant in our landscape flux time series.

Heaths and *Salix* fluxes

The heath class in this study includes both *Cassiope*, *Dryas*, and *Vaccinium* areas, and data from Christensen et al. (2000), Tagesson et al. (2013), and Jørgensen et al. (2015) are combined to calculate an average estimate for fluxes in these areas, which are held constant over time. Jørgensen et al. (2015) used different groups in their study, where different types of heath areas fall into "dry" and "moist" tundra (*Cassiope* and *Salix* heath). We calculated the weighted mean flux for each study for the heath class, and then we calculated a mean and pooled SE. Likewise, the *Salix* snowbed class was calculated in the same way as with heath, with data from the same three studies, but with only the flux from moist tundra from Jørgensen et al. (2015).

2.3.3 Combining data into landscape flux time series

The six combined surface classes occupy most of the study areas (Rylekærene and the valley floor, Table 1). This static areal coverage of the surface classes was calculated using QGIS v. 3.18.1 (QGIS.org, 2021).

The area-weighted flux was calculated for the two study areas, the valley floor and Rylekærene, with total areas of $15\,905\,003\,m^2$ and $1\,271\,303\,m^2$. This approach assumes no methane flux in the remaining 18.1 % and 3.7 % of the study areas, including the river, delta, and abrasion plateaus, as well as boulder fields in the "other" category in Table 1. The area-weighted landscape flux is calculated for each year, with fluxes in the fens and fen fringes being the only to change over time.

2.3.4 Fluxes in the gully area

In the recently eroded gully area, the fluxes in 2019 were calculated using the ordinary least square linear (OLS) regression described in Pirk et al. (2016a). Of the 113 measurements, 102 had a significant ($p < 0.05$) regression slope. The remaining 11 measurements were found on both the grassland areas and on recently eroded surfaces. They showed an increase in concentration over time close to zero, and they are interpreted as areas with no flux. The 11 measurements are included in the calculation of the mean flux of the recently eroded surfaces in the gully.

The mean flux and the standard error (SE) for all measurements were calculated by calculating the mean flux for repeated measurements for each plot. Further averaging for their respective surface class (gully, grasslands, fens) was done afterward, showing how fluxes can change in an area after an erosion event. Flux measurements from the gully area are limited to 10 d in the late growing season.

2.3.5 Valley flux and future impacts on methane emissions with increasing erosion activity

Recent active riverbank erosion in Zackenberg Valley raises the question of how the methane flux on a valley scale will change with increasing erosion in the future, and the sensitivity to such changes is explored below.

Changes in methane flux from increasing temperatures

In their study, Geng et al. (2019) compared the potential methane flux in the Zackenberg area modeled for the late 21st century with present-day conditions. They found an exponential growing season temperature–methane flux relationship based on Zackenberg and Kobbefjord data from 2008–2015. Present-day temperatures were modeled for the 1991–2010 period, and late 21st century temperatures were modeled for 2081–2100 under the Representative Concentration Pathway 8.5 (RCP8.5). Both present-day and future mean temperatures were modeled using the ECHAM5 general circulation model to limit the cold bias in the model, and the relative increase in methane flux was +141 % (Marilena Sophie Geng, personal communication, 24 April 2020). The relative increase ranges from +114 % to +171 % when considering the lower and upper 95 % confidence bounds; see Fig. 3 in Geng et al. (2019).

We assume a linear increase in valley methane flux of +141 % for this sensitivity study, ranging from +114 % to +171 % from 2016–2100, even though this period does not fully match the modeled periods, i.e., from 1991–2010 to 2081–2100.

Sensitivity to increasing erosion activity

We establish three pathways to quantify how erosion could affect the landscape flux in Zackenberg Valley. In the first pathway, we calculate the impact on the mean valley flux if the eroded areas are growing at an annual rate equivalent to the size of the recent gully ($720\,m^2\,yr^{-1}$). In the second and third pathway, the eroded area starts at $720\,m^2$ every year and grows to 5 and 10 times that area per year, respec-

tively, i.e., a linear increase over 85 years from $720\,\mathrm{m^2\,yr^{-1}}$ to $3600\,\mathrm{m^2\,yr^{-1}}$ and from $720\,\mathrm{m^2\,yr^{-1}}$ to $7200\,\mathrm{m^2\,yr^{-1}}$. In this calculation, the erosion can only occur in zones with excessive ice-rich permafrost near rivers and streams. To identify these zones, we use GIS data available from Cable et al. (2018). Inside our study area (Fig. 1), we identify parts of the landscape that likely have excess ice-rich top 1 m permafrost and are located near rivers, which include both rivers and tributaries; see Fig. 12 in Cable et al. (2018). Based on observations from the recent gully, erosion can occur up to 50 m from the rivers. Inside the identified zones, we model erosion of the size specified above and the fractional cover of surface classes. The reduction in mean flux for the eroded areas is subtracted from the landscape flux. As time goes, the eroded areas increase, causing larger impacts on the landscape flux, while all fluxes increase at the same rate as when the mean temperatures increase.

Revegetation of eroded areas

A similar gully in the northern part of the valley developed in 1999 (Christiansen et al., 2008), and it shows signs of revegetation on $\sim 40\,\%$ of the eroded areas to grassland after 20 years. This estimate is based on a visual interpretation of 100 points randomly scattered over eroded parts within the gully in an orthophoto from August 2019. From the estimate, we set the regrowth rate equal to $2\,\%\,\mathrm{yr^{-1}}$, and this rate of regrowth is included in the overall calculation.

3 Results

3.1 Environmental changes

Figure 3a shows the development of July–August soil and air temperatures since 1997 at 0.2 m depth and 2 m height measured at the climate station. The mean July–August temperature is $5.9\,°\mathrm{C}$ for air temperatures and $4.7\,°\mathrm{C}$ for the available soil temperatures. Air temperatures increased by $0.07\,°\mathrm{C\,yr^{-1}}$ (1997–2019, $n = 23$, Pearson's $r = 0.43$, $p = 0.04$), while no significant linear trend is observed in the soil temperature data during the same period. The timing of snowmelt in the study area (Fig. 3b) shows substantial variations between years, from 30 (DOY 150) to 27 July (DOY 208). During July and August, there is so far no clear trend toward drier or wetter conditions for both the heath areas (Fig. 3c) and the fens at the AC site (Fig. 3d) from the mid-2000s and forward. Measurements from chamber 6 show generally drier conditions than from chamber 1, which is located further out in the fen.

3.2 Timeline of methane fluxes from Rylekærene

Figure 4 summarizes the methane fluxes measured on fen and fen fringe (only AC 1 to 6) surface types in Zackenberg Valley during 17 growing seasons from 1997–2019. The

methane fluxes vary both between simultaneous measurements and between years. Fen fluxes generally show higher fluxes than those measured at the fen fringe, with mean fluxes ranging from 1.75 ± 0.27 to $8.3 \pm 0.31\,\mathrm{mg\,m^{-2}\,h^{-1}}$ in 1997 (Friborg et al., 2000) and 2000 (Joabsson and Christensen, 2001). Methane fluxes in the fen fringe ranged from $0.26 \pm 0.07\,\mathrm{mg\,m^{-2}\,h^{-1}}$ in 2011 to $3.41 \pm 0.57\,\mathrm{mg\,m^{-2}\,h^{-1}}$ in 2007 during July–August (Mastepanov et al., 2013, 2021).

3.3 Gully methane fluxes

Methane fluxes at exposed, eroded surfaces of the gully were different from the fluxes on the nearby, undisturbed surfaces (Fig. 5). The late growing season mean methane flux of the recently eroded surfaces in the gully in 2019 was $0.05 \pm 0.02\,\mathrm{mg\,m^{-2}\,h^{-1}}$, including positive and negative fluxes. The grassland surface cover in areas not disturbed by erosion shows a negative methane flux of $-0.06 \pm 0.01\,\mathrm{mg\,m^{-2}\,h^{-1}}$. The mean methane flux in the fen was $3.83 \pm 0.76\,\mathrm{mg\,m^{-2}\,h^{-1}}$, more than 75 times higher than the mean flux in the gully. For several plots in the fen, the flux was highly variable over time, reaching $20\,\mathrm{mg\,m^{-2}\,h^{-1}}$. Generally, the methane flux decreased with air temperature in the fen. In the gully, plots with patches of live vegetation showed mostly negative flux, while barren plots exhibited a positive flux. In the undisturbed grassland areas, vegetated and barren plot fluxes were negative. Methane emissions generally increased closer to the open water body of the nearby fen. The emergence of the gully changed the area from a small methane sink to a small source, following an initial substantial episodic release of methane stored in exposed ice in 2018 when the gully appeared (Christensen et al., 2020b).

3.4 Estimation of an integrated flux of methane in Zackenberg Valley

The July–August landscape flux of methane exposed large interannual variability over the valley floor and Rylekærene study areas over the 14 years, 2006–2019 (Fig. 6). The cumulative landscape fluxes and uncertainties are displayed as line plots and error bars overlapping stacked bar charts, which show the contribution from each of the six surface classes. Surface types with negative methane flux lower the landscape flux and SE for each of the surface classes on the stacked bar charts.

We observed no apparent trends for both areas ($n = 14$, Pearson's $r = -0.22$, $p = 0.44$) over the entire period. The mean flux for the 2006–2019 period in Rylekærene was $1.74 \pm 0.16\,\mathrm{mg\,m^{-2}\,h^{-1}}$ and $0.34 \pm 0.03\,\mathrm{mg\,m^{-2}\,h^{-1}}$ for the valley floor study area. Methane fluxes ranged from $0.98 \pm 0.11\,\mathrm{mg\,m^{-2}\,h^{-1}}$ in 2011 to $3.26 \pm 1.15\,\mathrm{mg\,m^{-2}\,h^{-1}}$ in 2007 in Rylekærene and from $0.17 \pm 0.05\,\mathrm{mg\,m^{-2}\,h^{-1}}$ to $0.67 \pm 0.23\,\mathrm{mg\,m^{-2}\,h^{-1}}$ for the valley floor. The two study
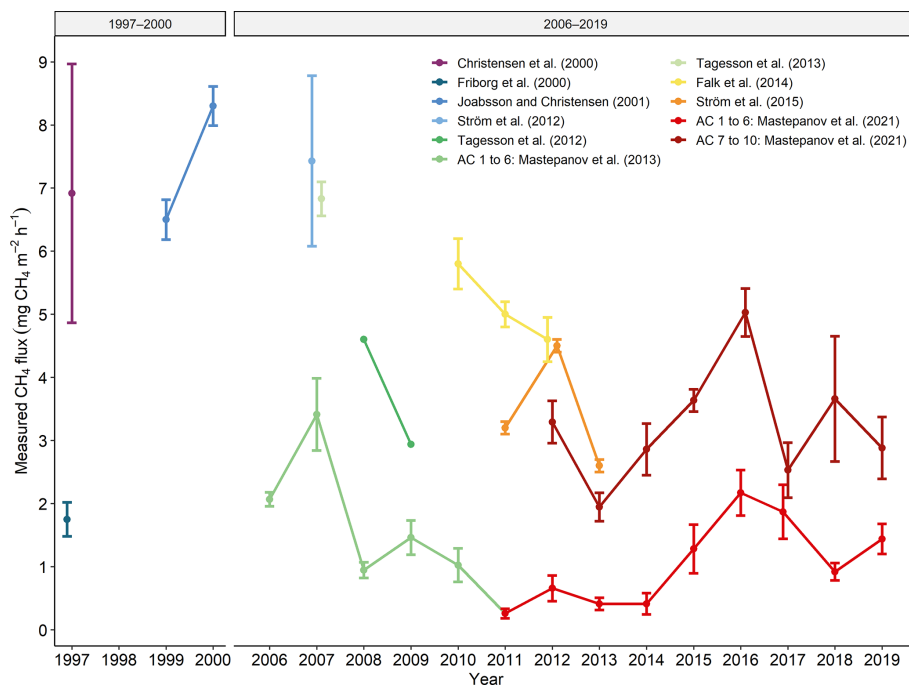
Figure 4. Timeline of methane fluxes measured during the growing season (1 July–31 August for AC) measured in fen areas (hummocky and continuous fen) and at the fringe of the fen (AC 1 to 6). Colors show different datasets. Please note that the years 2001–2005 are left out, as no published studies focusing on methane fluxes in undisturbed areas were made in this period. Also, note that points may be shifted slightly along the year axis to avoid overplotting.
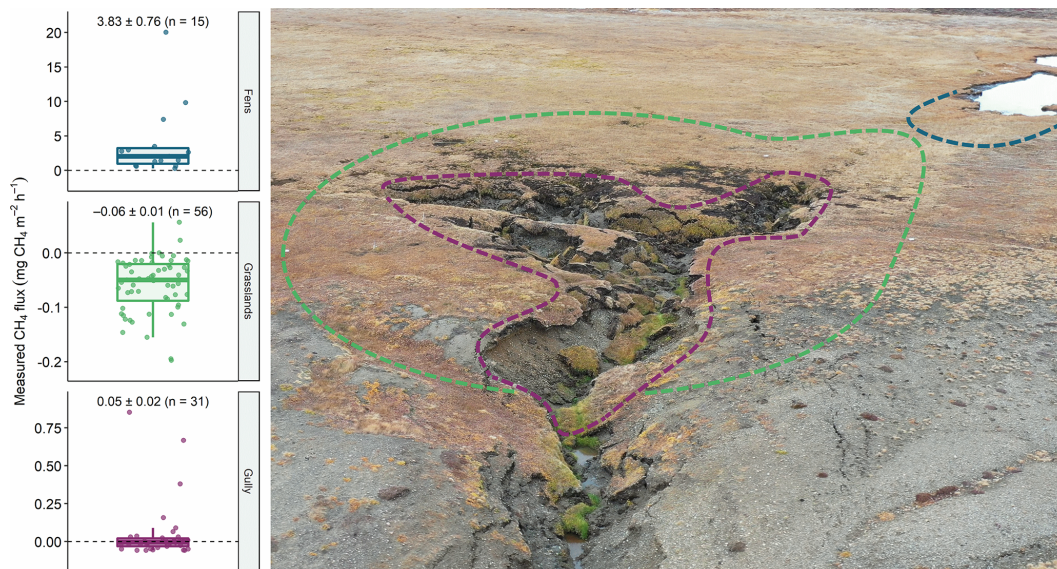

Figure 5. The gully and fen area near the Zackenberg Research Station. The three boxplots show the measured methane fluxes on different surface types between 23 August and 1 September 2019, when the image was captured. Dots on top of the boxplots show all the individual measurements. The dashed lines in the image indicate the approximate spatial extent of the measurements near the gully. The eroded area is ~ 50 m long and ~ 25 m at its widest, covering ~ 720 m^2.
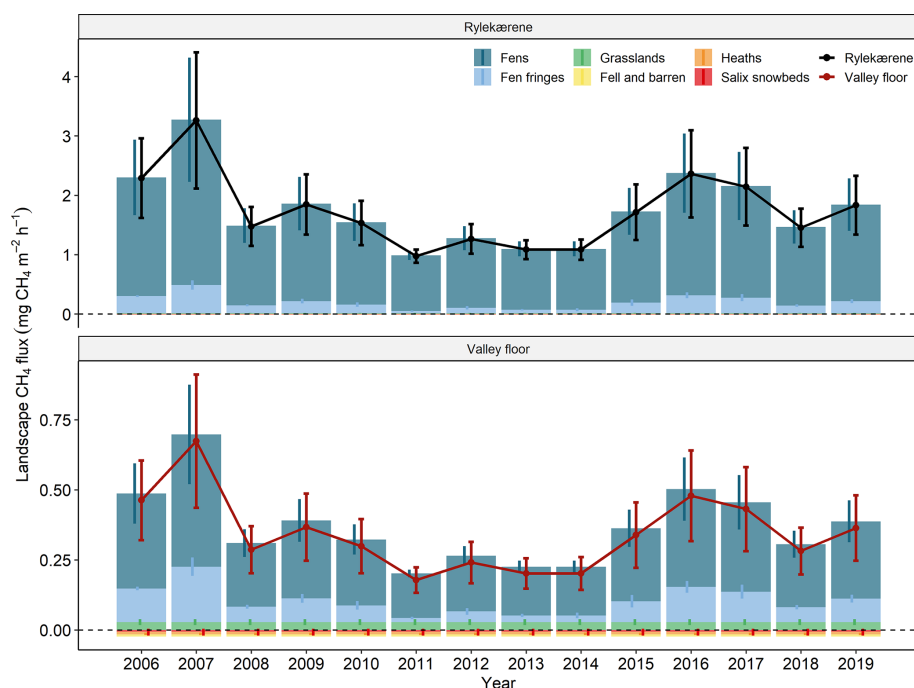
Figure 6. Cumulative fluxes and SE from the six surface classes are shown for the two areas. Fluxes and SE from each surface class are weighted to their relative coverage and shown with stacked bars. The fen and fen fringe fluxes are predominant in the calculation of both landscape fluxes, explaining the nearly identical pattern in interannual variability.

areas were net sources of methane throughout the period, although its magnitude changed significantly between years.

Areas with a high positive flux are, in relative terms, more dominant in Rylekærene than the valley floor, which instead has a more considerable negative flux from heaths, *Salix* snowbeds, and fell and barren areas, which decrease the mean landscape flux.

3.5 Methane emissions from the valley in a changing climate

The mean valley methane flux for July–August is calculated for 2016–2100, including the upper and lower bounds for the fluxes, when uncertainties from both the methane–temperature regression and the upscaling are combined (Fig. 7). For this comparison, mean fluxes are averaged over two periods, one for the mid-21st century (2041–2060) and another for the late-21st century (2081–2100). The mean landscape flux in the reference period (2008–2015) was $0.27 \, \text{mg} \, \text{m}^{-2} \, \text{h}^{-1}$ (Fig. 7a), while the mean flux from 2016–2019 (Fig. 7b) was $0.39 \, \text{mg} \, \text{m}^{-2} \, \text{h}^{-1}$. The modeled landscape flux without erosion (Fig. 7c) increases linearly over the century. Erosion rates of $720 \, \text{m}^2 \, \text{yr}^{-1}$ (Fig. 7d), 720–$3600 \, \text{m}^2 \, \text{yr}^{-1}$ (Fig. 7e), and 720–$7200 \, \text{m}^2 \, \text{yr}^{-1}$ (Fig. 7f) in the modeled flux all result in a net reduction in landscape flux, which becomes more pronounced over time. Higher rates of erosion result in a lower modeled flux for Zackenberg Valley.

When considering the differences between the fluxes shown in Fig. 7, the mid-century mean landscape flux could be reduced by up to $0.05 \, \text{mg} \, \text{m}^{-2} \, \text{h}^{-1}$, i.e., the difference between (Fig. 7c) and (Fig. 7f) corresponding to a reduction of 1.2 % of the landscape flux. Between 2081–2100, the reduction in methane flux for the most severe erosion pathway could be $0.029 \, \text{mg} \, \text{m}^{-2} \, \text{h}^{-1}$, equal to a reduction in the landscape flux of 4.9 %.

4 Discussion

4.1 Methane flux measurements

Several methane flux methods have been in use since the two first methane flux studies were carried out in 1997 (Fig. 4) in the Rylekærene area (Christensen et al., 2000; Friborg et al., 2000), including both manual chambers (Table 2) and EC measurements. Flux measurements over 14 years at AC show large interannual variability in methane fluxes even at a single site. Substantial spatial variability in fluxes is seen in Fig. 4 when studies are available in the same years. Differences in methane fluxes measured from these studies can be explained by site characteristics, equipment and sampling strategies, and both length and timing of the measurement period. Two studies are omitted in Fig. 4: Pirk et al. (2016b) studied the methane fluxes in the fen areas near the AC site under snow-covered conditions before the
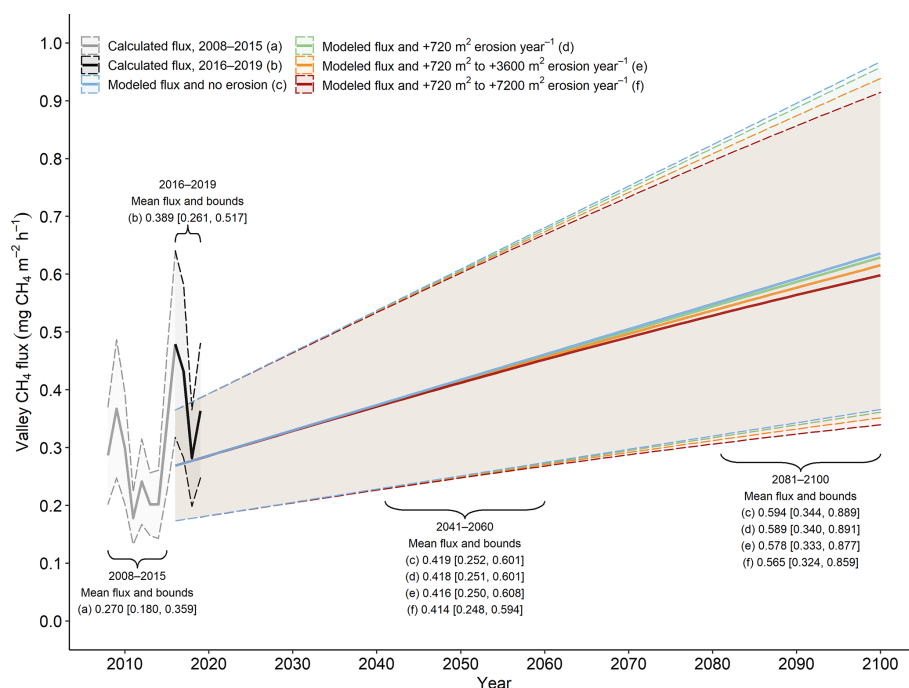
Figure 7. Methane fluxes in the valley floor study area increase over time if temperatures rise as modeled for the RCP8.5 scenario. However, increases in flux from rising temperatures are partly offset by erosion in the sensitivity study. Increasing erosion rates could reduce the mean flux of methane in the valley over time when a part of the landscape, a net source of methane, is converted into eroded areas with lower methane flux.

growing season in 2012 and 2014. Jørgensen et al. (2015) added flux measurements from 2012 covering only dry tundra (*Dryas* heath, abrasion plateau, and fell field) and moist tundra (*Salix* snowbeds and *Cassiope* heath) sites, both of them methane sinks. These findings exceeded the methane uptake on similar tundra surface classes in the area in Christensen et al. (2000). Higher soil and air temperatures in 2012 compared to 1997 could explain the higher fluxes (Fig. 3a), which also fits with relatively high methane uptake in 2007 when Tagesson et al. (2013) did their measurements on corresponding vegetation types. Spatial differences and the inclusion of unvegetated surfaces (abrasion plateau and fell field) and more advanced measurement equipment (Table 2) are other possible reasons for the larger uptake in Jørgensen et al. (2015).

Using a distributed manual chamber approach, Christensen et al. (2000) measured fluxes for an intensive study area, a part of Rylekærene, in 1997. In Fig. 4, only the combined measurements from hummocky and continuous fen plots are used. Alongside, Friborg et al. (2000) applied the EC method and found a much lower methane flux compared to Christensen et al. (2000) in approximately the same area. The fetch of the EC tower included surface classes with lower flux, which is a likely reason for lower mean flux Rylekærene reported in Friborg et al. (2000). The length of the measurement period was longer in Friborg et al. (2000), starting 1 June (Fig. 2), more than 3 weeks earlier than Christensen et

al. (2000), which further explains some of the differences as methane fluxes were low at the beginning of the measurement period. Christensen et al. (2000) measured methane fluxes two times per week per plot, while methane fluxes from EC were available every day for several weeks in July and August. The SE for the fen measurements in Christensen et al. (2000) in Fig. 4 is high due to the high flux variability within and between the two combined groups, hummocky and continuous fen.

Control plot flux measurements from Joabsson and Christensen (2001) are illustrated in Fig. 4 for a study site in the southern part of Rylekærene in 1999 and 2000. As shown in Table 2, the methods are comparable to Christensen et al. (2000), and the mean flux in both years is similar. The SEs are smaller, likely due to both fewer and less diverse plots, i.e., six continuous plots compared to a total of 18 hummocky and continuous plots in Christensen et al. (2000).

Two studies provide a basis for comparison in 2007, the growing season with the highest estimated landscape flux in the 14-year study period. Ström et al. (2012) and Tagesson et al. (2013) applied similar methods (Table 2), using plots near MM2 in the same year with comparable methane flux as a result. For Ström et al. (2012), the SE reported in Fig. 4 is comparatively high. This difference can be explained by the high SE associated with measurements of plots with high flux and high *Eriophorum scheuchzeri* coverage, combined with relatively low methane flux plots with low *Eriophorum*

scheuchzeri coverage. In Tagesson et al. (2013), measurements were done at 25 randomly placed plots in hummocky and continuous fen areas, which resulted in a lower SE for the combined fen classes. The key difference is the range of both high and low *Eriophorum scheuchzeri* plots in Ström et al. (2012) against the randomly selected placement in two fen classes in Tagesson et al. (2013).

In 2008 and 2009, Tagesson et al. (2012) combined gradient and EC methods to estimate methane fluxes. Their results for the two growing seasons show intermediate fluxes between the fluxes measured at the fen fringe and higher fluxes measured by chamber methods on fen surfaces. The size of the fluxes can be explained by the limited 43 % coverage of the fen surface class in the tower footprint for the prevailing wind direction in the growing season, while the rest of the footprint is covered by drier surface classes. Error estimates are not directly comparable with the other studies in Fig. 4. They are integrated over the entire measurement period and reported as total accumulated errors equal to 8 % and 12 % of the total flux in 2008 and 2009.

Based on control measurements in a continuous fen area during the growing seasons 2010–2012, Falk et al. (2014) reported mean methane fluxes larger than those measured at the fen fringe at the AC. Measurement methods are comparable to Ström et al. (2012) and Tagesson et al. (2013). They use an identical gas analyzer and similar measurement frequency. Different chamber sizes are used, but this is not expected to impact the measurements significantly, as chamber volumes are considered in the calculation of fluxes. Differences in mean flux between the 3 years were attributed to variable measurement periods in the 3 years and interannual variations in water level depth (Falk et al., 2014).

Ström et al. (2015) measured methane fluxes with the same approach as Falk et al. (2014). The main differences between the two studies are the timing and the site. The two sites are situated ∼ 600 m apart, which explains possible differences in fluxes due to water levels and substrate availability. Measurements in 2011 in Falk et al. (2014) began 14 d earlier, which may have caused some of the difference in mean fluxes. In 2012, fluxes were similar between the two studies. The two campaigns started one day apart in that year, indicating that conditions are similar despite the distance.

The outer four chambers of the AC installation show interannual variability in fluxes of a size similar to the manual chamber measurements of Falk et al. (2014), Ström et al. (2015), and EC measurements in Tagesson et al. (2012). The number of observations for chambers 7 to 10 is high (Table 3), and flux measurements from each chamber are available every 90 min during July and August. In some years, measurements are not available for the entire period. Differences in chamber fluxes may be explained by variability in water levels, but data are not available from the outermost chambers. Standard errors are higher due to relatively high variability in fluxes during the measurement period.

The previous studies show large differences in methane flux within the same fen ecosystem. Local spatial variability and interannual differences may explain these differences, and possibly also differences in methods.

Spatial variability in methane flux can be pronounced in tundra ecosystems with complex microtopography (Olefeldt et al., 2013) and differs significantly even at a meter scale (Fig. 4). Methane fluxes vary with local differences in substrate, water-table depth, grazing, vegetation composition, and productivity, each of which can either increase or limit the methane flux. Several of these interactions have been studied in Zackenberg Valley: increased substrate availability, mainly acetate, contributes to higher methane fluxes as shown by, e.g., Ström et al. (2003), while a low water table limits methane fluxes (Tagesson et al., 2013). Grazing can either decrease (Falk et al., 2014) or increase (Falk et al., 2015) the methane flux, depending on the vegetation cover. Vegetation composition and primary productivity are strong drivers of methane fluxes (Joabsson and Christensen, 2001; Ström et al., 2012, 2015).

Temporal variability in methane fluxes can be caused by differences in environmental parameters, both within a growing season and from one year to another. Soil temperature was found to explain less variability than species composition and primary productivity (Christensen et al., 2000; Ström et al., 2012), while soil temperatures showed a high correlation with methane flux within most individual years (Mastepanov et al., 2013). Late-lying snow delays the beginning of the growing season (Grøndahl et al., 2008), which controls several of the above-mentioned parameters. Only a few studies in Zackenberg Valley were conducted outside the growing season. However, the fall season could substantially impact the annual methane budget, mainly through emissions associated with the onset of soil freezing (Mastepanov et al., 2008). In contrast, wintertime (November–May) emissions may only have a limited impact on the annual methane budget (Pirk et al., 2016b).

Our analysis focuses on the mean of the July–August fluxes in the valley, but the automated chambers are running from snowmelt to the end of the field season (Fig. 2). The fixed period matches the timing of the previous studies, and the period showed a good representation of the mean flux of the entire measurement dataset. The first 30 to 40 d after snowmelt have been shown to express the main differences between years (Mastepanov et al., 2013), which is covered by the July–August mean fluxes to a large extent.

4.2 Combining flux measurements from multiple sources

Comparable mean methane fluxes across several existing studies indicate that the differences in methods and placement have an impact on the flux in fen areas. Differences arise mainly when measurement periods vary by several weeks and when measurement plots are distributed over sev-

eral different surface classes, i.e., hummocky and continuous fen. However, the fen fringe time series appears to express some of the variability in fluxes as the separate measurement campaigns when these are combined into one. Regression analysis shows a significant correlation between methane fluxes at chambers 1 to 6 and the grouped studies from the fen areas of Zackenberg Valley when pairing data for the same years. Deming regression is a reasonable choice of analysis when both the mean values of chamber 1 to 6 and the fen methane fluxes are associated with measurement errors and uncertainties. The composite fen dataset, made from six separate studies, increases the temporal coverage and the spatial coverage of the data used in the regression analysis. The SE of the calculated fluxes is estimated with jackknife resampling, providing a reasonable SE estimate for Deming regression (Linnet, 1990). When comparing flux data to OLS regression, the Deming regression slope is steeper. The steeper slope means that the estimated fen flux in 2007, when the flux was high, is $\sim 20\%$ higher when compared to OLS, which means that the difference in regression methods has a substantial impact on landscape fluxes.

Methane fluxes measured in chambers 1 to 6 are consistently lower than the fluxes in chambers 7 to 10. Therefore, data from chambers 1 to 6 are split into a separate surface class, the fen fringe. The addition of these lower flux fen areas impacts the landscape flux, but the width of the zone does most likely fluctuate across the valley. Here, 10 m is a simple estimate based on the situation at AC, but the width of the zone ultimately depends on the topographic gradient along the edge of the fens.

The remaining surface classes contribute with the same negative fluxes throughout the period, with a mean value representing each of the surface classes. Their net effect is offsetting some of the positive landscape methane flux, particularly for the valley floor. Several surface classes were studied in detail over a single growing season (Table 3), and the specific sites differ between studies. The fluxes from these areas are held constant due to a lack of more detailed data, and fluxes from different studies are averaged into a single mean flux, which represents a range of sites and environmental conditions. We omitted surface flux data from the grasslands, measured by Christensen et al. (2000). The measured mean flux was significantly higher at $2.1 \pm 1.6\,\mathrm{mg\,m^{-2}\,h^{-1}}$, and the measurement site was located near the border of the fen (see Fig. 2 in Christensen et al., 2000), making the data more comparable to the fen fringe than the grasslands surface class.

Manual measurements in the gully area were limited to 10 d in the late growing season. Still, the size of the mean fluxes is in good agreement with the concurrent fluxes measured at AC 7 to 10 (Mastepanov et al., 2021) and the grassland flux reported in Tagesson et al. (2013). Negative fluxes were measured on plots with patchy vegetation in the gully, while mineral-rich plots had low positive fluxes of methane. The highest methane emissions in the gully were found on

two unvegetated plots, located where the gully had recently eroded (up to $0.85\,\mathrm{mg\,m^{-2}\,h^{-1}}$). These sparse observations suggest a considerable reduction in flux on eroded gully surfaces over time when limited organic soils remain in the gully.

4.3 Methane flux upscaling

Vegetation plot measurement on the dominant vegetation classes combined with long-term AC site data from 2006–2019 enables the calculation of landscape flux time series for Rylekærene and the valley floor. This approach is more direct than modeling based on physical parameters that have otherwise been shown to correlate well with methane flux for Rylekærene (Tagesson et al., 2013). However, a limitation of the approach is its lack of a dynamic component, which could take spatial differences across the valley into account, e.g., snow cover or changing soil moisture conditions from one year to another, affecting the valley floor and the AC site differently.

Both Christensen et al. (2000) and Tagesson et al. (2013) found a significant difference in the methane flux in hummocky and continuous fen areas in Rylekærene and treated the two groups separately. These groups were combined in this study to match the existing valley-wide surface cover classification. Comparing the mean flux found for Rylekærene shows good agreement between the flux estimates in this study and the fluxes reported in Tagesson et al. (2013). Four growing seasons (2007–2010) are common for the two studies, and in three of the seasons, the flux estimates of this study lie within the model uncertainty in Tagesson et al. (2013). The one notable exemption is 2007 mean flux ($3.26 \pm 1.15\,\mathrm{mg\,m^{-2}\,h^{-1}}$) in this study, and it differs a lot from the $1.6 \pm 1.0\,\mathrm{mg\,m^{-2}\,h^{-1}}$ modeling result in Tagesson et al. (2013). The difference can be explained with a relatively high flux measured at the AC site in a year without extreme temperature or moisture conditions in the valley (Fig. 2), which are central parameters in the modeling of Tagesson et al. (2013).

The AC site is located by the outlet of the Rylekærene fen. The flow of water through the area affects the water level at the site, which is shown in Fig. 3d. Water level data were measured manually, once per day in the growing season, between 2006–2019 near the outermost of the six original chambers (chamber 1). Automatic water level measurements are available for chamber 1 and chamber 6, the innermost chamber, in the 2010–2019 period, with a gap in data for 2013. For July–August, water levels are generally lower at the innermost chamber but show variability similar to the water levels measured further out in the fen. Water level measurements are not available for the outer four chambers.

The changing water level may control the methane flux and explain its high variability 2006–2019, but neither water levels, air temperatures, nor soil temperatures correlate significantly (p-value threshold of 0.05) with methane when

analyzing the interannual variability for July–August mean values. Over the 14 years, p values range from 0.29 to 0.56. The lack of correlation over the time series illustrates a complex interaction between methane and environmental conditions when analyzed on a decadal scale. Figure 4 shows the methane flux of previous studies, which mainly focused on wetter parts of the fen where the flux is high. The flux appears to vary relatively less over time further out in the fen, as the soil moisture conditions change less between years than the chambers 1 to 6 at the AC site. One example is the smaller relative variability at chambers 7 to 10. The smaller, discontinuous fen areas seen in Fig. 1 are characterized by a less stable inflow of water than Rylekærene, which may therefore cause high interannual variability in the transition zones between different vegetation types.

Christensen et al. (2000) based their study of Zackenberg Valley methane flux on chamber measurements from a $\sim 0.1\,\mathrm{km^2}$ area of the northern part of Rylekærene (Fig. 1). The methane flux was measured with chambers on the five dominant vegetation types, and a mean flux for the valley was calculated by scaling fluxes to match the land cover classification of Bay (1998). The upscaled methane flux for the entire valley floor was $1.9 \pm 0.7\,\mathrm{mg\,m^{-2}\,h^{-1}}$, which is higher than in any of the years in this study, which range from 0.18 ± 0.05 and $0.67 \pm 0.24\,\mathrm{mg\,m^{-2}\,h^{-1}}$. The distribution of land cover classes differs slightly between Bay (1998) and the HyMap dataset. Still, a primary cause for the much higher valley estimate is the higher measured fluxes in the widespread grassland class with a flux of $2.9 \pm 1.6\,\mathrm{mg\,m^{-2}\,h^{-1}}$ in Christensen et al. (2000), compared to $0.1 \pm 0.04\,\mathrm{mg\,m^{-2}\,h^{-1}}$ (SE converted from SD) in Tagesson et al. (2013), the source of the grassland flux data used in our study. This difference impacts the valley flux, and if we substitute only the grassland-type flux from 0.1 to $2.9\,\mathrm{mg\,m^{-2}\,h^{-1}}$ in the upscaling to the entire valley floor, it would at least double the methane flux in the valley.

Jørgensen et al. (2015) found a relatively high methane uptake on dry tundra in 2012, e.g., *Salix* snowbeds and heath surfaces, compared to what has been found earlier. When including the uptake from Jørgensen et al. (2015), the valley flux is reduced, but the effect could vary between years with larger sinks in dry, warm years, as these surface classes combined account for more than 40 % of the valley floor (Table 1). Soil temperatures were lower in 2012 than in 2007 in July–August, which does not explain the higher uptake on dry tundra soils in 2012, indicating that some dry tundra surfaces have a higher methane uptake than others. Additionally, flux data from 2007 are used for both heath, grassland, and *Salix* snowbed surface classes. While flux measurements in the fen areas were exceptionally high in that year, this was not the case for the drier surface types. Landscape fluxes from both the valley floor and Rylekærene are highly variable between years and do not show an increasing trend from the available data. Both study areas show the same pattern, but the areal distribution between classes differs, mak-

ing the Rylekærene study area almost entirely dependent on the variability of only the fen and fen fringe surface types. In the larger valley floor study area, grassland, *Salix* snowbeds, heaths, and fell and barren surface classes dampen the variability between years.

Zackenberg Valley shows the potential for increased methane fluxes in the 21st century, as methane shows a positive correlation with temperatures (Geng et al., 2019), similar to the rest of Greenland and the Arctic (AMAP, 2017).

Landscape-scale methane flux estimations are available from other subarctic and tundra sites (Table 4) in North America, Scandinavia, and Russia. The upscaled growing season fluxes range from $0.5\,\mathrm{km^2}$, extending from covering a few different ecosystems in a single site (Christensen et al., 2004) to large-scale estimates of fluxes covering up to $320\,000\,\mathrm{km^2}$ for the Hudson Bay Lowlands (Roulet et al., 1994). Mean methane fluxes in these landscapes range from 0.3 to $3\,\mathrm{mg\,m^{-2}\,h^{-1}}$ across different scales and landscape types, covering growing seasons of variable length with studies scattered across several decades. The mean methane flux for Zackenberg Valley from 2006–2019 is $0.34\,\mathrm{mg\,m^{-2}\,h^{-1}}$ in the valley floor area ($\sim 16\,\mathrm{km^2}$) and $1.74\,\mathrm{mg\,m^{-2}\,h^{-1}}$ in the fen-rich Rylekærene area ($\sim 1.3\,\mathrm{km^2}$). Hence, the results from Zackenberg Valley are in good agreement with observations from comparable studies at other sites. However, the two Zackenberg study areas are smaller than most studies listed in Table 4. All the included studies are either fully or partly based on chamber measurements and upscaling with areal coverage of the surface classes, making them comparable to this study. Several studies (Bartlett et al., 1992; Roulet et al., 1994; Bosse and Frenzel, 2001; Hartley et al., 2015) estimated the landscape methane fluxes based on observations from a single year. The remaining studies combine observations from multiple years or studies to a flux estimate from each surface cover class (Christensen et al., 2004; Schneider et al., 2009; Andresen et al., 2017; Morozumi et al., 2019). Flux measurements from several years lead to more robust landscape flux estimates, as the fluxes are highly variable between years.

The large differences in study area size and composition ultimately determine the mean methane flux estimates of the landscape, making direct comparisons between sites difficult. For instance, the mean landscape flux found in this study is nearly 5 times greater for the fen-rich Rylekærene study area, which is fully contained in the valley floor study area. On an even larger scale, the entire northeast of Greenland acts as a net sink of methane, as Jørgensen et al. (2015) found a mean methane flux of $\sim -0.08\,\mathrm{mg\,m^{-2}\,h^{-1}}$ in their $10\,675\,\mathrm{km^2}$ study area.

Several other studies have applied the EC method for ecosystem methane flux measurements on a landscape scale in the Arctic, e.g., Fan et al. (1992), Sachs et al. (2008), Wille et al. (2008), Jackowicz-Korczynski et al. (2010), Parmentier et al. (2011), and Taylor et al. (2018). While the EC method requires less workload and integrates ecosystem fluxes at

Table 4. Comparison of landscape-integrated growing season methane flux for various subarctic and Arctic sites with a minimum size of $0.5\,\text{km}^2$.

Publication	Location	Climate zone	Landscape type	Mean flux ($\text{mg CH}_4\,\text{m}^{-2}\,\text{h}^{-1}$)	Area size (km^2)
Bartlett et al. (1992)	Yukon–Kuskokwim Delta (Alaska, USA)	Subarctic	Wetlands	1.8	97 400
Roulet et al. (1994)	Hudson Bay Lowlands (Ontario-Manitoba, Canada)	Subarctic	Wetlands	0.8	320 000
Bosse and Frenzel (2001)	Yenisey River (W Siberia, Russia)	Subarctic	Mire, wetlands, and pine forest	1	361
Christensen et al. (2004)	Stordalen (Norrbotten, Sweden)	Subarctic	Mire	2.7 to 3.0	0.5
Heikkinen et al. (2004)	Lek Vorkuta (N Komi, Russia)	Arctic tundra	Heath, peatland, and *Salix*	0.6	114
Schneider et al. (2009)	Lena Delta (N Siberia, Russia)	Arctic tundra	Wetlands	0.4	29 036
Hartley et al. (2015)	Kevo (Lapland, Finland)	Subarctic	Aapa mires and birch forest	0.3 to 0.4	100
Andresen et al. (2017)	Utqiaġvik Peninsula (Alaska, USA)	Arctic tundra	Arctic coastal plains	0.6	1779
Morozumi et al. (2019)	Indigirka (NE Siberia, Russia)	Arctic tundra	Larch forest, shrubs, and wetlands	1.6	96

high temporal resolution by nonintrusive means (McGuire et al., 2012), those studies are generally restricted to smaller areas less than $0.5\,\text{km}^2$. Ecosystem fluxes from these studies range between ~ 0.1 and $6.2\,\text{mg m}^{-2}\,\text{h}^{-1}$, with the lowest growing season fluxes measured at an upland tussock tundra site by Eightmile Lake in Alaska (Taylor et al., 2018) and the highest fluxes measured in a mire in Stordalen, north Sweden (Jackowicz-Korczynski et al., 2010). Mean growing season fluxes found in Zackenberg using the EC method are within this range (Friborg et al., 2000; Tagesson et al., 2012).

4.4 Landscape methane flux in a changing climate

A warming trend in both air and soil temperatures has been observed for Zackenberg Valley (Abermann et al., 2017; Christensen et al., 2020b). The increase in temperatures has contributed to the destabilization of permafrost, leading to several active periglacial landforms in recent years (Docherty et al., 2017; Cable et al., 2018; Christensen et al., 2020b). Modeling results show higher soil temperatures and a deepening of the AL in Zackenberg Valley in the future (Christiansen et al., 2008; Westermann et al., 2015). Increasing temperatures are expected to impact both positive and negative methane flux and surface erosion in the Arctic (Schuur et al., 2015; Geng et al., 2019; Oh et al., 2020), which is also likely for Zackenberg Valley. The emergence of several active erosion sites in Zackenberg Valley in recent years

could be an initial step towards increased erosion activity during the 21st century. In 2019, after the disappearance of methane-rich ice wedges in the previous year, carbon-rich soils had been washed out from the gully, leaving a silt–organic mix with limited potential for methane emission in the area (Christensen et al., 2020b). Our study defines three erosion pathways to illustrate the sensitivity of methane flux to land cover changes on a valley scale. We hypothesize large-scale linear growth in eroded areas in parts of the valley that are likely to have a high ground ice content and are located near streams and rivers identified by Cable et al. (2018). These erosion areas are assumed to share the characteristics of those observed in the gully area in 2019. Increased gully erosion could transform large areas with surfaces with both methane emission and uptake into well-drained, low-emission eroded surfaces. These erosion pathways are unlikely, but they are valuable as a sensitivity study illustrating the difference in importance of increasing temperatures relative to eroding surfaces.

Even large-scale erosion on the valley floor would have a limited impact on the mean methane flux, reducing it by up to 1.2 % on average between 2041–2060 for the most extreme erosion pathway (Fig. 7f). The reduction becomes more pronounced (4.9 % reduction) between 2081–2100, as eroded areas would continue to erode at a faster pace. Disturbances of this magnitude are comparable to the size of

the edge trimming during the GLOF in 2017 in the lower river section (Tomczyk et al., 2020), located inside the valley floor study area. The impact on fluxes from one added gully, similar in size to the recent gully per year, is minimal (less than 1 % reduction) at the end of the 21st century (Fig. 7d) when compared to the uncertainty range. In our calculation of landscape methane fluxes after erosion, eroded areas become revegetated at a rate of 2 % yr^{-1}. This rate may change over time and from one location to another, dependent on species composition and soil conditions in the eroded areas. The change is assumed to be linear in this case but may accelerate over time, as plant communities established. In the calculation, revegetated areas were considered to have the same methane flux as the grasslands in the gully area. Limited data from the measurements in the gully area show that the undisturbed vegetated areas take up slightly more methane than the disturbed vegetation patches in the gully, but the 10 d measurement period did not allow for more detailed measurements on temporal dynamics in the area.

The resulting changes in flux following erosion, particularly for the less extreme pathways (Fig. 7d and e), are minor relative to the considerable uncertainty in the general shift in methane for the valley following an increase in temperature. The mean methane flux is shown in Fig. 7 with a wide uncertainty range, partly caused by a lack of perfect fit between fluxes and temperatures and the uncertainties in the estimated landscape fluxes in Fig. 6. The variability between years in this study is substantial. The mean valley flux for 2016–2019 exceeds the confidence bounds, which shows that this should be seen as a sensitivity study of changes occurring on decadal scales.

In this case, methane fluxes were measured in a gully, which becomes more drained with a loss of organic soils from the surface after an erosion event (Christensen et al., 2020b).

The gully described in this study has likely formed as a direct consequence of pronounced lateral erosion from the river, which steepened the gully, allowing for increased drainage of water and sediments. The increased drainage exposed more and more of the ice wedges and frozen soils, which later thawed and flowed out through the steeper gully. Lateral erosion of a similar scale has not been recorded to occur along the smaller rivers and streams in Zackenberg, but several smaller erosion sites have been described in recent years (Docherty et al., 2017; Cable et al., 2018). The gully shares characteristics with thermokarst gullies, a common type of thermokarst erosion, including extent, depth, and shape (Jorgenson et al., 2008). Abrupt thaw, including both gullies and thermokarst areas, can take different forms and affect the surface methane flux through disturbances in both vegetation and hydrology (Turetsky et al., 2020). Olefeldt et al. (2016) describe thermokarst landscapes, which include thermo-erosion gullies characterized by lateral movement of sediments, similar to the gully described in our study. Olefeldt et al. (2016) estimate that ∼ 20 % of land areas in the

northern permafrost zone are thermokarst landscapes, meaning they are either currently characterized by soil settlement or erosion or prone to developing into thermokarst landforms in the future. Thermokarst landforms have diverse impacts on a landscape, dependent on their type (Kokelj and Jorgenson, 2013). They could form abruptly and rapidly responding to increasing temperatures (Farquharson et al., 2019; Lewkowicz and Way, 2019). Wickland et al. (2020) found a 42 % increase in growing season methane flux from 1949–2018 in a wet polygonal tundra after an increase in thermokarst erosion of ice wedges. Thermokarst lakes cover large areas across the boreal zone and in the Arctic and have been reported to be substantial emitters of methane (Wik et al., 2016; Walter Anthony et al., 2018; Engram et al., 2020). The findings from thermokarst lakes contrast the results from this study, where erosion causes draining and loss of organic material (Fig. 5). Wik et al. (2016) found a mean flux, combining diffusion and ebullition, of ∼ 3.7 mg m^{-2} h^{-1} from thermokarst lakes in the ice-free season. Walter Anthony et al. (2018) found an accelerating increase in methane fluxes from thermokarst lakes in their modeling of methane in the 21st century for the circumpolar region, which shows that the impacts on methane in the event of erosion are diverse. It should be noted that there is a difference in the receiving end of the gully formation between our study and these thermokarst lake studies as the drainage in the Zackenberg Valley goes into the river systems with few or no stagnant reservoirs between.

5 Conclusions

In this study, we have summarized 14 measurement years of methane fluxes and several short-term campaigns, which provide a unique insight into the large variability in methane fluxes in a high-Arctic-tundra landscape of Zackenberg Valley. We have combined July–August measurements from a monitoring site running from 2006–2019 with detailed measurements of the most common vegetation types in the valley to estimate valley-wide methane fluxes over the period. For the valley, the net emission of methane in July–August shows differences by nearly a factor of 4 between individual years (2006–2019). Consistently dry or wet surfaces may remain relatively stable in terms of methane fluxes over the period, as indicated by the data from previous site-specific campaigns in the valley. However, the large areas covering the boundary between these hosts highly variable methane fluxes, significantly impacting methane fluxes on a landscape scale. Future multi-year campaigns should focus on measuring the full gradient from wet fens to dry heath to improve estimations of landscape methane fluxes, as the fluxes from different surface classes may respond differently to changes in environmental conditions, such as moisture, temperature, and snow cover.

Observations from recently eroded gully revealed a small source of methane in this type of landscape. Rapid export of carbon-rich soils and an effective drainage system in the gully are likely the main reasons for the limited methane fluxes.

With rising temperatures in Zackenberg Valley, methane emissions are expected to increase drastically during the 21st century. The warming increases permafrost thaw, which could increase surface erosion in the valley. When compared, our findings show the increase in methane emission from undisturbed fen areas has a much larger impact on the valley-wide fluxes than surface erosion. Increased erosion could offset some of the rise in methane fluxes from the valley, but this would require large-scale impacts on vegetated surfaces.

This study shows the importance of multi-year methane monitoring with wide spatial coverage, as interannual variability is substantial when considering a full composite landscape even in a single valley in the Arctic.

Code and data availability. Data from the GEM ClimateBasis and GeoBasis Zackenberg subprograms used in this paper are free and open data, available at https://data.g-e-m.dk/ (last access: 27 June 2021, registration needed). The data are licensed with terms of use under the Creative Commons CC-BY-SA license. Processed data and scripts used for the analyses are available from the corresponding author upon reasonable request. Direct links to the GEM data sources are listed in the following.

AC water level automatic: https://doi.org/10.17897/mj7b-z461 (Greenland Ecosystem Monitoring, 2021a).

AC water level manual: https://doi.org/10.17897/6hcp-m521 (Greenland Ecosystem Monitoring, 2021b).

Air temperature, 200 cm – 60 min average: https://doi.org/10.17897/xv96-hc57 (Greenland Ecosystem Monitoring, 2021c).

Flux monitoring – AC: https://doi.org/10.17897/430p-ds31 (Greenland Ecosystem Monitoring, 2021d).

Mix-1 soil moisture: https://doi.org/10.17897/ennb-t831 (Greenland Ecosystem Monitoring, 2021e).

Snow cover (central area): https://doi.org/10.17897/499c-h459 (Greenland Ecosystem Monitoring, 2021f).

Soil temperature, 20 cm – 60 min average: https://doi.org/10.17897/xw7c-na36 (Greenland Ecosystem Monitoring, 2021g).

References

Abermann, J., Hansen, B., Lund, M., Wacker, S., Karami, M., and Cappelen, J.: Hotspots and key periods of Greenland climate change during the past six decades, Ambio, 46, 3–11, https://doi.org/10.1007/s13280-016-0861-y, 2017.

AMAP: AMAP assessment 2015: Methane as an Arctic climate forcer, Arctic Monitoring and Assessment Programme (AMAP), Oslo, Norway, Oslo, Norway, 152 pp., 2015.

AMAP: Snow, Water and Permafrost in the Arctic (SWIPA) 2017, Oslo, Norway, 269 pp., 2017.

Andresen, C. G., Lara, M. J., Tweedie, C. E., and Lougheed, V. L.: Rising plant-mediated methane emissions from arctic wetlands, Glob. Change Biol., 23, 1128–1139, https://doi.org/10.1111/gcb.13469, 2017.

Bartlett, K. B., Crill, P. M., Sass, R. L., Harriss, R. C., and Dise, N. B.: Methane emissions from tundra environments in the Yukon-Kuskokwim delta, Alaska, J. Geophys. Res., 97, 16645–16660, https://doi.org/10.1029/91jd00610, 1992.

Bay, C.: Vegetation mapping of Zackenberg valley, northeast Greenland, Danish Polar Center and Botanical Museum, University of Copenhagen, 1998.

Bosse, U. and Frenzel, P.: CH_4 emissions from a West Siberian mire, Suo, 52, 99–114, 2001.

Cable, S., Christiansen, H. H., Westergaard-Nielsen, A., Kroon, A., and Elberling, B.: Geomorphological and cryostratigraphical analyses of the Zackenberg Valley, NE Greenland and significance of Holocene alluvial fans, Geomorphology, 303, 504–523, https://doi.org/10.1016/j.geomorph.2017.11.003, 2018.

Christensen, T. R.: Methane emission from Arctic tundra, Biogeochemistry, 21, 117–139, https://doi.org/10.1007/bf00000874, 1993.

Christensen, T. R.: Climate science: Understand Arctic methane variability, Nature, 509, 279–281, https://doi.org/10.1038/509279a, 2014.

Christensen, T. R., Friborg, T., Sommerkorn, M., Kaplan, J., Illeris, L., Søgaard, H., Nordstrøm, C., and Jonasson, S.: Trace gas exchange in a high-arctic valley 1. Variations in CO_2 and CH_4 flux between tundra vegetation types, Global Biogeochem. Cy., 14, 701–713, https://doi.org/10.1029/1999gb001134, 2000.

Christensen, T. R., Johansson, T. R., Akerman, H. J., Mastepanov, M., Malmer, N., Friborg, T., Crill, P., and Svens-

son, B. H.: Thawing sub-arctic permafrost: Effects on vegetation and methane emissions, Geophys. Res. Lett., 31, L04501, https://doi.org/10.1029/2003gl018680, 2004.

Christensen, T. R., Arndal, M. F., and Topp-Jørgensen, E.: Greenland Ecosystem Monitoring Annual Report Cards 2019, DCE – Danish Centre for Environment and Energy, Aarhus University, Aarhus, Denmark, 40 pp., 2020a.

Christensen, T. R., Lund, M., Skov, K., Abermann, J., López-Blanco, E., Scheller, J., Scheel, M., Jackowicz-Korczynski, M., Langley, K., Murphy, M. J., and Mastepanov, M.: Multiple Ecosystem Effects of Extreme Weather Events in the Arctic, Ecosystems, 24, 122–136, https://doi.org/10.1007/s10021-020-00507-6, 2020b.

Christiansen, H. H., Sigsgaard, C., Humlum, O., Rasch, M., and Hansen, B. U.: Permafrost and Periglacial Geomorphology at Zackenberg, in: High-Arctic Ecosystem Dynamics in a Changing Climate, Advances in Ecological Research, 151–174, Amsterdam, the Netherlands, 2008.

COWI: eBee saves the day: mapping Greenland's Zackenberg Research Station, available at: https://www.sensefly.com/app/uploads/2017/11/eBee_saves_day_mapping_greenlands_zackenberg_research_station.pdf (last access: 23 June 2021), 2015.

Crill, P. M., Bartlett, K. B., Harriss, R. C., Gorham, E., Verry, E. S., Sebacher, D. I., Madzar, L., and Sanner, W.: Methane flux from Minnesota peatlands, Global Biogeochem. Cy., 2, 371–384, https://doi.org/10.1029/gb002i004p00371, 1988.

Docherty, C. L., Hannah, D. M., Riis, T., Leth, S. R., and Milner, A. M.: Large thermo-erosional tunnel for a river in northeast Greenland, Polar Sci., 14, 83-87, https://doi.org/10.1016/j.polar.2017.08.001, 2017.

Ehhalt, D. H.: The atmospheric cycle of methane, Tellus, 26, 58–70, https://doi.org/10.3402/tellusa.v26i1-2.9737, 1974.

Elberling, B., Tamstorf, M. P., Michelsen, A., Arndal, M. F., Sigsgaard, C., Illeris, L., Bay, C., Hansen, B. U., Christensen, T. R., Hansen, E. S., Jakobsen, B. H., and Beyens, L.: Soil and Plant Community-Characteristics and Dynamics at Zackenberg, in: Advances in Ecological Research: High-Arctic Ecosystem Dynamics in a Changing Climate, Elsevier, Amsterdam, the Netherlands, 223–248, 2008.

Engram, M., Anthony, K. M. W., Sachs, T., Kohnert, K., Serafimovich, A., Grosse, G., and Meyer, F. J.: Remote sensing northern lake methane ebullition, Nat. Clim. Change, 10, 511–517, https://doi.org/10.1038/s41558-020-0762-8, 2020.

Falk, J. M., Schmidt, N. M., and Ström, L.: Effects of simulated increased grazing on carbon allocation patterns in a high arctic mire, Biogeochemistry, 119, 229–244, https://doi.org/10.1007/s10533-014-9962-5, 2014.

Falk, J. M., Schmidt, N. M., Christensen, T. R., and Ström, L.: Large herbivore grazing affects the vegetation structure and greenhouse gas balance in a high arctic mire, Environ. Res. Lett., 10, 045001, https://doi.org/10.1088/1748-9326/10/4/045001, 2015.

Fan, S. M., Wofsy, S. C., Bakwin, P. S., Jacob, D. J., Anderson, S. M., Kebabian, P. L., McManus, J. B., Kolb, C. E., and Fitzjarrald, D. R.: Micrometeorological measurements of CH_4 and CO_2 exchange between the atmosphere and subarctic tundra, J. Geophys. Res., 97, 16627–16643, https://doi.org/10.1029/91jd02531, 1992.

Farquharson, L. M., Romanovsky, V. E., Cable, W. L., Walker, D. A., Kokelj, S. V., and Nicolsky, D.: Climate Change Drives Widespread and Rapid Thermokarst Development in Very Cold Permafrost in the Canadian High Arctic, Geophys. Res. Lett., 46, 6681–6689, https://doi.org/10.1029/2019gl082187, 2019.

Friborg, T., Christensen, T. R., Hansen, B. U., Nordstrøm, C., and Søgaard, H.: Trace gas exchange in a high-Arctic valley 2. Landscape CH_4 fluxes measured and modeled using eddy correlation data, Global Biogeochem. Cy., 14, 715–723, https://doi.org/10.1029/1999gb001136, 2000.

Geng, M. S., Christensen, J. H., and Christensen, T. R.: Potential future methane emission hot spots in Greenland, Environ. Res. Lett., 14, 035001, https://doi.org/10.1088/1748-9326/aaf34b, 2019.

Greenland Ecosystem Monitoring: GeoBasis Zackenberg – Hydrology – AC_Water_level_automatic, Greenland Ecosystem Monitoring [data set], https://doi.org/10.17897/MJ7B-Z461, 2021a.

Greenland Ecosystem Monitoring: GeoBasis Zackenberg – Hydrology – AC_Water_level_manual, Greenland Ecosystem Monitoring [data set], https://doi.org/10.17897/6HCP-M521, 2021b.

Greenland Ecosystem Monitoring: ClimateBasis Zackenberg – Air temperature – Air temperature, 200 cm @ 60 min sample (°C), Greenland Ecosystem Monitoring [data set], https://doi.org/10.17897/XV96-HC57, 2021c.

Greenland Ecosystem Monitoring: GeoBasis Zackenberg – Flux monitoring – AC, Greenland Ecosystem Monitoring [data set], https://doi.org/10.17897/430P-DS31, 2021d.

Greenland Ecosystem Monitoring: GeoBasis Zackenberg – Soil properties – Mix-1_Soil_moisture, Greenland Ecosystem Monitoring [data set], https://doi.org/10.17897/ENNB-T831, 2021e.

Greenland Ecosystem Monitoring: GeoBasis Zackenberg – Snow properties – Snow cover (Central area), Greenland Ecosystem Monitoring [data set], https://doi.org/10.17897/499C-H459, 2021f.

Greenland Ecosystem Monitoring: ClimateBasis Zackenberg – Soil temperature – Soil temperature, 20 cm – 60 min average (°C), Greenland Ecosystem Monitoring [data set], https://doi.org/10.17897/XW7C-NA36, 2021g.

Grøndahl, L., Friborg, T., Christensen, T. R., Ekberg, A., Elberling, B., Illeris, L., Nordstrøm, C., Rennermalm, Å., Sigsgaard, C., and Søgaard, H.: Spatial and inter-annual variability of trace gas fluxes in a heterogeneous high-arctic landscape, in: Advances in Ecological Research: High-Arctic Ecosystem Dynamics in a Changing Climate, Elsevier, Amsterdam, the Netherlands, 473–498, 2008.

Hartley, I. P., Hill, T. C., Wade, T. J., Clement, R. J., Moncrieff, J. B., Prieto-Blanco, A., Disney, M. I., Huntley, B., Williams, M., Howden, N. J. K., Wookey, P. A., and Baxter, R.: Quantifying landscape-level methane fluxes in subarctic Finland using a multiscale approach, Glob. Change Biol., 21, 3712–3725, https://doi.org/10.1111/gcb.12975, 2015.

Heikkinen, J. E. P., Virtanen, T., Huttunen, J. T., Elsakov, V., and Martikainen, P. J.: Carbon balance in East European tundra, Global Biogeochem. Cy., 18, GB1023, https://doi.org/10.1029/2003gb002054, 2004.

IPCC: Climate Change The IPCC Scientific Assessment, Intergovernmental Panel on Climate Change, Cambridge, 1990.

Jackowicz-Korczynski, M., Christensen, T. R., Bäckstrand, K., Crill, P., Friborg, T., Mastepanov, M., and Ström, L.: Annual cy-

cle of methane emission from a subarctic peatland, J. Geophys. Res., 115, G02009, https://doi.org/10.1029/2008jg000913, 2010.

Joabsson, A. and Christensen, T. R.: Methane emissions from wetlands and their relationship with vascular plants: an Arctic example, Glob. Change Biol., 7, 919–932, https://doi.org/10.1046/j.1354-1013.2001.00044.x, 2001.

Jorgenson, M. T., Schur, Y. L., and Osterkamp, T. E.: Thermokarst in Alaska, Ninth International Conference on Permafrost, Fairbanks, 869–876, 2008.

Jørgensen, C. J., Lund Johansen, K. M., Westergaard-Nielsen, A., and Elberling, B.: Net regional methane sink in High Arctic soils of northeast Greenland, Nat. Geosci., 8, 20–23, https://doi.org/10.1038/ngeo2305, 2015.

Knoblauch, C., Beer, C., Liebner, S., Grigoriev, M. N., and Pfeiffer, E.-M.: Methane production as key to the greenhouse gas budget of thawing permafrost, Nat. Clim. Change, 8, 309–312, https://doi.org/10.1038/s41558-018-0095-z, 2018.

Kokelj, S. V. and Jorgenson, M. T.: Advances in Thermokarst Research, Permafrost Periglac. Process., 24, 108–119, https://doi.org/10.1002/ppp.1779, 2013.

Lewkowicz, A. G. and Way, R. G.: Extremes of summer climate trigger thousands of thermokarst landslides in a High Arctic environment, Nat. Commun., 10, 1329, https://doi.org/10.1038/s41467-019-09314-7, 2019.

Linnet, K.: Estimation of the linear relationship between the measurements of two methods with proportional errors, Stat. Med., 9, 1463–1473, https://doi.org/10.1002/sim.4780091210, 1990.

Livingston, G. and Hutchinson, G.: Enclosure-based measurement of trace gas exchange: applications and sources of error, in: Biogenic trace gases: measuring emissions from soil and water, edited by: Matson, P. A. A. H., R.C., Blackwell Science Ltd., 14–51, Amsterdam, the Netherlands, 1995.

López-Blanco, E., Jackowicz-Korczynski, M. A., Mastepanov, M., Skov, K., Westergaard-Nielsen, A., Williams, M., and Christensen, T.: Multi-year data-model evaluation reveals the importance of nutrient availability over climate in arctic ecosystem C dynamics, Environ. Res. Lett., 15, 094007, https://doi.org/10.1088/1748-9326/ab865b, 2020.

Mastepanov, M., Sigsgaard, C., Dlugokencky, E. J., Houweling, S., Ström, L., Tamstorf, M. P., and Christensen, T. R.: Large tundra methane burst during onset of freezing, Nature, 456, 628–630, https://doi.org/10.1038/nature07464, 2008.

Mastepanov, M., Sigsgaard, C., Tagesson, T., Ström, L., Tamstorf, M. P., Lund, M., and Christensen, T. R.: Revisiting factors controlling methane emissions from high-Arctic tundra, Biogeosciences, 10, 5139–5158, https://doi.org/10.5194/bg-10-5139-2013, 2013.

Mastepanov, M., Pirk, N., Lopez-Blanco, E., Skov, K., Rudd, D., Jackowicz-Korczynski, M., Tamstorf, M., Scheller, J., and Christensen, T. R.: Fifteen years of methane flux measurements in high-arctic tundra, in preparation, 2021.

McGuire, A. D., Christensen, T. R., Hayes, D., Heroult, A., Euskirchen, E., Kimball, J. S., Koven, C., Lafleur, P., Miller, P. A., Oechel, W., Peylin, P., Williams, M., and Yi, Y.: An assessment of the carbon balance of Arctic tundra: comparisons among observations, process models, and atmospheric inversions, Biogeosciences, 9, 3185–3204, https://doi.org/10.5194/bg-9-3185-2012, 2012.

Meltofte, H. and Rasch, M.: The Study Area at Zackenberg, in: Advances in Ecological Research: High-Arctic Ecosystem Dynamics in a Changing Climate, Elsevier, Amsterdam, the Netherlands, 101–110, 2008.

Meltofte, H., Christensen, T. R., Elberling, B., Forchhammer, M. C., and Rasch, M.: Introduction, in: Advances in Ecological Research: High-Arctic Ecosystem Dynamics in a Changing Climate, Elsevier, Amsterdam, the Netherlands, 1–12, 2008.

Morozumi, T., Shingubara, R., Suzuki, R., Kobayashi, H., Tei, S., Takano, S., Fan, R., Liang, M., Maximov, T., and Sugimoto, A.: Estimating methane emissions using vegetation mapping in the taiga–tundra boundary of a north-eastern Siberian lowland, Tellus B, 71, 1581004, https://doi.org/10.1080/16000889.2019.1581004, 2019.

Morrissey, L. A. and Livingston, G. P.: Methane emissions from Alaska Arctic tundra: An assessment of local spatial variability, J. Geophys. Res.-Atmos., 97, 16661–16670, https://doi.org/10.1029/92jd00063, 1992.

Nisbet, E. G., Manning, M. R., Dlugokencky, E. J., Fisher, R. E., Lowry, D., Michel, S. E., Myhre, C. L., Platt, M., Allen, G., Bousquet, P., Brownlow, R., Cain, M., France, J. L., Hermansen, O., Hossaini, R., Jones, A. E., Levin, I., Manning, A. C., Myhre, G., Pyle, J. A., Vaughn, B. H., Warwick, N. J., and White, J. W. C.: Very Strong. Atmospheric Methane Growth in the 4 Years 2014–2017: Implications for the paris Agreement, Global Biogeochem. Cy., 33, 318–342, https://doi.org/10.1029/2018gb006009, 2019.

Oh, Y., Zhuang, Q. L., Liu, L. C., Welp, L. R., Lau, M. C. Y., Onstott, T. C., Medvigy, D., Bruhwiler, L., Dlugokencky, E. J., Hugelius, G., D'Imperio, L., and Elberling, B.: Reduced net methane emissions due to microbial methane oxidation in a warmer Arctic, Nat. Clim. Change, 10, 317–321, https://doi.org/10.1038/s41558-020-0734-z, 2020.

Olefeldt, D., Turetsky, M. R., Crill, P. M., and McGuire, A. D.: Environmental and physical controls on northern terrestrial methane emissions across permafrost zones, Glob. Change Biol., 19, 589–603, https://doi.org/10.1111/gcb.12071, 2013.

Olefeldt, D., Goswami, S., Grosse, G., Hayes, D., Hugelius, G., Kuhry, P., McGuire, A. D., Romanovsky, V. E., Sannel, A. B., Schuur, E. A., and Turetsky, M. R.: Circumpolar distribution and carbon storage of thermokarst landscapes, Nat. Commun., 7, 13043, https://doi.org/10.1038/ncomms13043, 2016.

Parmentier, F., Van Huissteden, J., Van Der Molen, M., Schaepman-Strub, G., Karsanaev, S., Maximov, T., and Dolman, A.: Spatial and temporal dynamics in eddy covariance observations of methane fluxes at a tundra site in northeastern Siberia, J. Geophys. Res., 116, G03016, https://doi.org/10.1029/2010jg001637, 2011.

Pedersen, S. H., Tamstorf, M. P., Abermann, J., Westergaard-Nielsen, A., Lund, M., Skov, K., Sigsgaard, C., Mylius, M. R., Hansen, B. U., Liston, G. E., and Schmidt, N. M.: Spatiotemporal Characteristics of Seasonal Snow Cover in Northeast Greenland from in Situ Observations, Arct. Antarctic Alp. Res., 48, 653–671, https://doi.org/10.1657/aaar0016-028, 2016.

Pirk, N., Mastepanov, M., Parmentier, F.-J. W., Lund, M., Crill, P., and Christensen, T. R.: Calculations of automatic chamber flux measurements of methane and carbon dioxide using short time series of concentrations, Biogeosciences, 13, 903–912, https://doi.org/10.5194/bg-13-903-2016, 2016a.

Pirk, N., Tamstorf, M. P., Lund, M., Mastepanov, M., Pedersen, S. H., Mylius, M. R., Parmentier, F. J. W., Christiansen, H. H., and Christensen, T. R.: Snowpack fluxes of methane and carbon dioxide from high Arctic tundra, J. Geophys. Res.-Biogeo., 121, 2886–2900, https://doi.org/10.1002/2016jg003486, 2016b.

QGIS.org: QGIS Geographic Information System v. 3.18.1, Open Source Geospatial Foundation Project, 2021.

R Core Team: R: A language and environment for statistical computing v. 4.0.2, R Foundation for Statistical Computing, 2021.

Roulet, N. T., Jano, A., Kelly, C., Klinger, L., Moore, T., Protz, R., Ritter, J., and Rouse, W.: Role of the Hudson Bay lowland as a source of atmospheric methane, J. Geophys. Res.-Atmos., 99, 1439–1454, https://doi.org/10.1029/93jd00261, 1994.

Sachs, T., Wille, C., Boike, J., and Kutzbach, L.: Environmental controls on ecosystem-scale CH_4 emission from polygonal tundra in the Lena River Delta, Siberia, J. Geophys. Res., 113, G00A03, https://doi.org/10.1029/2007jg000505, 2008.

Schneider, J., Grosse, G., and Wagner, D.: Land cover classification of tundra environments in the Arctic Lena Delta based on Landsat 7 ETM+ data and its application for upscaling of methane emissions, Remote Sens. Environ., 113, 380–391, https://doi.org/10.1016/j.rse.2008.10.013, 2009.

Schuur, E. A., McGuire, A. D., Schadel, C., Grosse, G., Harden, J. W., Hayes, D. J., Hugelius, G., Koven, C. D., Kuhry, P., Lawrence, D. M., Natali, S. M., Olefeldt, D., Romanovsky, V. E., Schaefer, K., Turetsky, M. R., Treat, C. C., and Vonk, J. E.: Climate change and the permafrost carbon feedback, Nature, 520, 171–179, https://doi.org/10.1038/nature14338, 2015.

Shakhova, N., Semiletov, I., Leifer, I., Sergienko, V., Salyuk, A., Kosmach, D., Chernykh, D., Stubbs, C., Nicolsky, D., Tumskoy, V., and Gustafsson, Ö.: Ebullition and storm-induced methane release from the East Siberian Arctic Shelf, Nat. Geosci., 7, 64–70, https://doi.org/10.1038/ngeo2007, 2014.

Stiegler, C., Lund, M., Christensen, T. R., Mastepanov, M., and Lindroth, A.: Two years with extreme and little snowfall: effects on energy partitioning and surface energy exchange in a high-Arctic tundra ecosystem, The Cryosphere, 10, 1395–1413, https://doi.org/10.5194/tc-10-1395-2016, 2016.

Ström, L., Ekberg, A., Mastepanov, M., and Christensen, T. R.: The effect of vascular plants on carbon turnover and methane emissions from a tundra wetland, Glob. Change Biol., 9, 1185–1192, https://doi.org/10.1046/j.1365-2486.2003.00655.x, 2003.

Ström, L., Tagesson, T., Mastepanov, M., and Christensen, T. R.: Presence of Eriophorum scheuchzeri enhances substrate availability and methane emission in an Arctic wetland, Soil Biol. Biochem., 45, 61–70, https://doi.org/10.1016/j.soilbio.2011.09.005, 2012.

Ström, L., Falk, J. M., Skov, K., Jackowicz-Korczynski, M., Mastepanov, M., Christensen, T. R., Lund, M., and Schmidt, N. M.: Controls of spatial and temporal variability in CH_4 flux in a high arctic fen over three years, Biogeochemistry, 125, 21–35, https://doi.org/10.1007/s10533-015-0109-0, 2015.

Svensson, B. H. and Rosswall, T.: In situ Methane Production from Acid Peat in Plant Communities with Different Moisture Regimes in a Subarctic Mire, Oikos, 43, 341–350, https://doi.org/10.2307/3544151, 1984.

Søgaard, H., Nordstrøm, C., Friborg, T., and Hansen, B. U.: Trace gas exchange in a high-arctic valley 3. Integrating and scaling CO_2 fluxes from canopy to landscape using flux data, footprint modeling, and remote sensing, Global Biogeochem. Cy., 14, 725–744, https://doi.org/10.1029/1999gb001137, 2000.

Søndergaard, J., Tamstorf, M., Elberling, B., Larsen, M. M., Mylius, M. R., Lund, M., Abermann, J., and Rigét, F.: Mercury exports from a High-Arctic river basin in Northeast Greenland (74° N) largely controlled by glacial lake outburst floods, Sci. Total Environ., 514, 83–91, https://doi.org/10.1016/j.scitotenv.2015.01.097, 2015.

Tagesson, T., Molder, M., Mastepanov, M., Sigsgaard, C., Tamstorf, M. P., Lund, M., Falk, J. M., Lindroth, A., Christensen, T. R., and Ström, L.: Land-atmosphere exchange of methane from soil thawing to soil freezing in a high-Arctic wet tundra ecosystem, Glob. Change Biol., 18, 1928–1940, https://doi.org/10.1111/j.1365-2486.2012.02647.x, 2012.

Tagesson, T., Mastepanov, M., Mölder, M., Tamstorf, M. P., Eklundh, L., Smith, B., Sigsgaard, C., Lund, M., Ekberg, A., Falk, J. M., Friborg, T., Christensen, T. R., and Ström, L.: Modelling of growing season methane fluxes in a high-Arctic wet tundra ecosystem 1997–2010 using in situ and high-resolution satellite data, Tellus B, 65, https://doi.org/10.3402/tellusb.v65i0.19722, 2013.

Taylor, M. A., Celis, G., Ledman, J. D., Bracho, R., and Schuur, E. A. G.: Methane Efflux Measured by Eddy Covariance in Alaskan Upland Tundra Undergoing Permafrost Degradation, J. Geophys. Res.-Biogeo., 123, 2695–2710, https://doi.org/10.1029/2018jg004444, 2018.

Thornton, B. F., Prytherch, J., Andersson, K., Brooks, I. M., Salisbury, D., Tjernström, M., and Crill, P. M.: Shipborne eddy covariance observations of methane fluxes constrain Arctic sea emissions, Sci. Adv., 6, eaay7934, https://doi.org/10.1126/sciadv.aay7934, 2020.

Tomczyk, A. M. and Ewertowski, M. W.: UAV-based remote sensing of immediate changes in geomorphology following a glacial lake outburst flood at the Zackenberg river, northeast Greenland, J. Maps, 16, 86–100, https://doi.org/10.1080/17445647.2020.1749146, 2020.

Tomczyk, A. M., Ewertowski, M. W., and Carrivick, J. L.: Geomorphological impacts of a glacier lake outburst flood in the high arctic Zackenberg River, NE Greenland, J. Hydrol., 591, 125300, https://doi.org/10.1016/j.jhydrol.2020.125300, 2020.

Turetsky, M. R., Abbott, B. W., Jones, M. C., Anthony, K. W., Olefeldt, D., Schuur, E. A. G., Grosse, G., Kuhry, P., Hugelius, G., Koven, C., Lawrence, D. M., Gibson, C., Sannel, A. B. K., and McGuire, A. D.: Carbon release through abrupt permafrost thaw, Nat. Geosci., 13, 138–145, https://doi.org/10.1038/s41561-019-0526-0, 2020.

Walter Anthony, K., Schneider von Deimling, T., Nitze, I., Frolking, S., Emond, A., Daanen, R., Anthony, P., Lindgren, P., Jones, B., and Grosse, G.: 21st-century modeled permafrost carbon emissions accelerated by abrupt thaw beneath lakes, Nat. Commun., 9, 3262, https://doi.org/10.1038/s41467-018-05738-9, 2018.

Westermann, S., Elberling, B., Højlund Pedersen, S., Stendel, M., Hansen, B. U., and Liston, G. E.: Future permafrost conditions along environmental gradients in Zackenberg, Greenland, The Cryosphere, 9, 719–735, https://doi.org/10.5194/tc-9-719-2015, 2015.

Whalen, S. C. and Reeburgh, W. S.: A methane flux time series for tundra environments, Global Biogeochem. Cy., 2, 399–409, https://doi.org/10.1029/gb002i004p00399, 1988.

Wickland, K. P., Jorgenson, M. T., Koch, J. C., Kanevskiy, M., and Striegl, R. G.: Carbon dioxide and methane flux in a dynamic Arctic tundra landscape: Decadal-scale impacts of ice-wedge degradation and stabilization, Geophys. Res. Lett., 47, e2020GL089894, https://doi.org/10.1029/2020gl089894, 2020.

Wik, M., Varner, R. K., Anthony, K. W., MacIntyre, S., and Bastviken, D.: Climate-sensitive northern lakes and ponds are critical components of methane release, Nat. Geosci., 9, 99–106, https://doi.org/10.1038/ngeo2578, 2016.

Wille, C., Kutzbach, L., Sachs, T., Wagner, D., and Pfeiffer, E. M.: Methane emission from Siberian arctic polygonal tundra: eddy covariance measurements and modeling, Glob. Change Biol., 14, 1395–1408, https://doi.org/10.1111/j.1365-2486.2008.01586.x, 2008.